Preliminary Propulsion System Sizing Methods for PEM Fuel Cell Aircraft

Daniel Juschus

Technische Universiteit Delft

TU Delft

Preliminary Propulsion System Sizing Methods for PEM Fuel Cell Aircraft

by

Daniel Juschus

to obtain the degree of Master of Science
at the Delft University of Technology,
to be defended publicly on Friday the 29th of October 2021 at 14:15.

Student number:	4439317	
Project duration:	3rd of September 2020 – 29th of October 2021	
Thesis committee:	Dr. ir. G. la Rocca,	TU Delft, Chair
	Dr. F. Oliviero,	TU Delft, Responsible Thesis Supervisor
	S. Taylor	GKN Aerospace, Company Supervisor
	Dr. F. Yin,	TU Delft, Examiner

An electronic version of this thesis is available at `http://repository.tudelft.nl/`.

TU Delft

In memory of Prof. Pim Groen

Summary

Fuel cell (FC) aircraft are one of the most promising technological solutions for the first generation of sustainable aircraft, especially for short and medium ranges. A FC uses hydrogen from a tank and oxygen from the surrounding air to produce water and electricity, the latter of which is then used by electric motors to power the aircraft through propellers. Of the many types of FCs that exist, so-called proton-exchange membrane (PEM) FCs are the most suitable for transport applications. The main advantages include a quick start-up due to its low operating temperature below 100°C, lightweight and compact design and a high technical readiness level, having been applied for example in trains or busses.

A FC propulsion system consists of a stack, which is where the electrochemical reaction takes place, and several supporting subsystems, called collectively the balance of plant (BOP). For a large vehicle operating at high altitudes, the BOP consists of at least three parts: 1. the electrically driven centrifugal compressor, to increase the inlet air pressure, 2. the liquid cooling system, of which the main part is the heat exchanger and 3. the humidifier. All of these components are grouped together in a so-called FC engine, which also contains an electric motor and a propeller. Multiple of these are then placed on the wing or the fuselage. Furthermore, due to the lower power density of FC systems, which is in the order of magnitude of 1 kW/kg, a battery should be added, effectively making a FC aircraft a hybrid one. The FC system is then sized for cruise and the battery, which is placed either in the fuselage or the wing, takes care of any additional power requirements. In a wider sense, the liquid hydrogen tank, which is placed behind the passengers, is a part of the propulsion system as well.

An important part of the implementation of such a new technology is the development of sizing and design methods, especially for the early design phases. Regarding FC aircraft, only very little research is available, particularly regarding generalised methods. One particular deficiency, on which the focus is place in this thesis, is the imbalance in the level of detail between the performance and the weight estimation. Whereas the former often consists of analytical models, the latter is usually only accounted for by using a constant value for the specific power of the whole system. The goal of this thesis is to address this research gap by developing a set of methods for the preliminary sizing of PEMFC propulsion systems for CS-25 aircraft. There are two important things to notice at this point: 1. no such aircraft have flown yet, meaning that there is essentially no data, which is why the modelling approach will have to be based on physics, and 2. at the level of detail required here, the weight and performance estimations become so entangled that both must be addressed simultaneously.

In the sizing process of the FC system, the cell model is first run, which determines the cell voltage as well as its efficiency. Next is an internal iteration loop, which is required due to the compressor, as it is the only part of the system which directly consumes some amount of power. This means that the stack needs to produce both this power, as well as the propulsive one, requiring a convergence between both components. From this electrical output power of the stack, various other parameters such as the heat rate or the mass flow of air are derived, which are then used as inputs for the remaining models. For each BOP, an existing modelling approach from literature is used, but with a number of simplifying assumptions. For the mass estimation, the physical design of each component is considered, for instance with the length of the tubes in the heat exchanger, the thickness of the membrane of the humidifier or the diameter of the compressor. Due to the complex geometry of the latter, a CAD model is generated within the sizing process. Finally, the stack model is run, where the total number of cells and the area per cell are determined using the system voltage and required power output respectively. The mass of the stack then follows from these parameters, given certain materials and thicknesses for its various parts.

A major amount of time was also spent in this thesis to integrate the Python FC system sizing script described in the paragraph above into an aircraft sizing environment, in order to demonstrate its suitability for this purpose. The choice was made to use the Initiator, an in-house Matlab tool. The Initiator performs the preliminary sizing procedure of any CS-25 aircraft. It also includes a hybrid branch, which was used here. Given that a FC propulsion system corresponds to serial-hybrid configuration, the gas turbine was replaced in the code with the FC system and the gearbox and generator were removed. Most of the modules of the hybrid sizing process were further modified. For instance, in the fuselage configurator, a very simple tank dimensioning procedure was used, and the fuselage was stretched. Most importantly, the FC system sizing process is run in the Class 2 module. This module determines the MTOM from a detailed OEM estimation and takes the remaining masses from the Class 1 estimation. The latter performs a wing/power loading constraint as well as a mission analysis.

The first part of the results presented in this report are in relation to a sizing study that was performed using an existing regional turboprop aircraft, the ATR 72-600, as a reference. The original mission parameters and general requirements were used as an input to the Initiator. First, a corresponding conventional aircraft was sized using the hybrid branch, to verify its accuracy. While the empty mass (OEM) and wing loading showed a really close match, the difference in the maximum power and fuel mass were higher. Regarding the FC-powered ATR, the maximum take-off mass (MTOM) increases by 69%, which is mostly due to the OEM, which increased by 132%. This in turn is mostly caused by the heavy FC engines, weighing slightly more than 8 tons, which is considerably more than the 964 kg of the original turboprop engines. Furthermore, the fuselage is extended by 4.3 m to make space for the tank. Even though these results might seem discouraging at first, one must keep in mind that this aircraft can fly the same mission as the original and that the increased mass by itself is not necessarily a problem.

The second part of the results consists of several sensitivity studies, conducted both on the level of the FC system and of the entire aircraft. First, two important subsystem design parameters were examined: the compressor pressure ratio β and the cell oversizing factor. A higher β leads to a heavier compressor, as expected. Its positive effect on the stack in terms of an increase in efficiency is negated by an increase in power required. For the oversizing factor, an increase results in a higher stack mass due to the reduced power density, but reduces the masses of the other BOP components. For both, it is important to note that the fuel mass is affected as well, meaning that the optimisation of such parameters can only happen at the level of the complete aircraft. Next, it was examined how the system behaves if no compressor is present. As expected, all masses increase significantly. This means that while the compressor might not necessarily be required to provide sea-level pressure, it is still overall useful.

In the final section, the effect of several mission parameters on the entire aircraft was examined using the ATR 72 example. The variation of the range resulted in an increase in the fuel mass (which is low to begin with due to the higher energy density of hydrogen), but not in the battery mass, as this component is not active during cruise. This result shows that in some ways, a FC aircraft is much less sensitive to the range requirement than a purely battery-powered one. Next, the take-off distance was examined, as this is the sizing constraint for the battery at the original design point (i.e. the battery is not sized by its energy requirement). However, with a slight increase in the distance, this changed, suddenly altering the situation. This shows that the optimisation process of such a propulsion system is a complex procedure, as the effect of all parameters must be kept in mind.

It can be concluded that the main research goal was achieved, as the resulting FC system model was applied successfully to an aircraft sizing scenario as well as several sensitivity studies. Through the results, it was demonstrated how such a more detailed approach enables new analysis capabilities in relation to important aspects of the design of FC aircraft. Therefore, this thesis projects presents an important step in the development of generalised sizing & design methods for FC aircraft, thereby making a small contribution to the first generation of truly sustainable aircraft.

Preface

This thesis project marks the conclusion of my journey to obtain a Master of Science degree in Aerospace Engineering from the TU Delft. The report which lies in front of you contains a detailed summary of all the work that I performed in the last year, starting with a description of the propulsion system model that I developed and finishing with a presentation of the results obtained with this model, as well as a critical reflection. Any reader who is knowledgeable in topics such as aircraft design and propulsion, as well as aerospace engineering in general, should be able to follow. Previous knowledge regarding fuel cells is not strictly necessary, as I did my best to provide a suitable introduction.

I'm grateful that I was given the opportunity to do my thesis on the topic that I'm most interested in, and that I have focussed on for the past few years: the design of fuel cell aircraft. During my DSE (our final Bachelor project), I understood for the first time that fuel cells are a viable option for the coming generation of sustainable aircraft. The immense success we achieved during that project was partially thanks to the tireless supervision of Professor Pim Groen, who sadly passed away during this thesis project.

I would also like to explain the choice for the cover image, which I took many years ago, as I arrived in Iceland for the first time. One of the most formative experiences of my life with regard to climate change was my second visit to a glacier in Iceland, which had at that point receded by what felt like hundreds of meters, compared to when I saw it for the first time, leaving behind nothing but a sad remnant of its former glory. This only motivated me further in my desire to contribute to making flying truly sustainable, which had been one of the biggest motivations for my studies right from the beginning.

On a positive note, I'm excited about the fact that in the past few years, several promising commercial projects for sustainable aircraft have emerged. These have been brought to life not only by start-ups, but also by big players in the industry. As such, it was great to do this thesis in connection with the H2GEAR project by GKN Aerospace, which aims to develop a fuel cell propulsion system for a sub-regional aircraft. As the next step, I'm excited to start my professional career in the pursuance of my long-standing goal: making flying sustainable.

Completing a Master thesis is not an easy task by itself, but has been an even bigger challenge during this global pandemic. As for most students, my life was affected massively. Therefore, I would like to thank, with my whole heart, those close friends, from Delft as well as from home, who supported me in these times in addition to, of course, my parents. I would also like to thank my two supervisors: Fabrizio Oliviero from the TU Delft and Simon Taylor from GKN Aerospace. Finally, I would like to express my gratitude to several other people who have helped me with their expert knowledge in various fields, namely Joe from GKN Aerospace and Matteo, Maurice and Giuseppe from the faculty of Aerospace Engineering.

Daniel Juschus
Delft, October 2021

Contents

List of Figures

List of Tables

Nomenclature

List of Acronyms

Acronym	Meaning
AEO	All engines operating
BM	Battery mass
BOP	Balance of plant
BP	Bipolar plate
CAD	Computer-aided design
CG	Centre of gravity
EM	Electric Motor
EP	Endplate
FC	Fuel cell
FM	Fuel mass
GB	Gearbox
GDL	Gas diffusion layer
GT	Gas turbine
HHV	Higher heating value
HX	Heat exchanger
LG	Landing gear
LT	Low temperature
MEA	Membrane electrode assembly
MTOM	Maximum take-off mass
OEI	One engine inoperative
OEM	Operational empty mass
OEMexBat	Operational empty mass excluding the battery mass
PEM	Proton-exchange membrane
PM	Power management
ROC	Rate of climb
RPM	Revolutions per minute
SAF	Sustainable aviation fuel
SL	Sea level
SOFC	Solid oxide fuel cell
TO	Take-off
TRL	Technical readiness level
UAV	Unmanned aerial vehicle

List of Symbols

Symbol	Meaning	Units
A	Area	m^2
b	Blade height	m
c	Mass transport loss constant	V
c	Absolute velocity	m/s
c_p	Specific heat capacity	J/(kg K)
D	Diameter	m
D_W	Diffusivity of water in air	m^2/s
d	Depth	m
E	Electric potential	V
F	Faraday constant	C/mol
h	Specific enthalpy	J/kg
h	Height	m
j	Current density	A/m^2
l	Length	m
M	Molar mass	kg/mol
$\dot{m}$	Mass flow	kg/s
n	Number of (channels)	-
P	Power	W
p	Pressure	atm
p	Power density	W/m^2
Q	Volumetric flow	m^3/s
$\dot{Q}$	Heat rate	W
R	Gas constant	J/(mol K)
r	Area specific resistance	$\Omega\ m^2$
T	Temperature	K
t	Thickness	m
u	Peripheral speed	m/s
V	Voltage	V
v	Velocity	m/s
w	Relative velocity	m/s
w	Width	m
α	Transfer coefficient	-
α	Absolute flow angle	rad
α	Heat transfer coefficient	$W/(m^2\ K)$
β	Compressor pressure ratio	-
β	Relative flow angle	rad
η	Efficiency	-
λ	Stoichiometric ratio	-
μ_f	Fuel utilisation factor	-
ρ	Material density	kg/m^3
ρ_{MEA}	Area density of MEA	kg/m^2
τ	Time	s
Φ	Supplied power ratio	-
ξ	Throttle parameter	-
ω	Humidity ratio	-

List of Subscripts[1]

Subscript	Meaning(s)
0	Standard conditions / exchange / HX inlet
1	Inlet of rotor or HX tubes or humidifier dry side
2	Outlet of rotor or HX tubes or humidifier dry side
2,s	Inlet of stator
3	Outlet of stator / inlet of humidifier wet side
4	Outlet of humidifier wet side
c	Cell
b	Inside HX tubes
bat	Battery
comb	Combined
comp	Compressor
d	Diffusion
e	Electric output of stack
f	Fuel
h	Hub
leak	Leakage
limit	Limiting
loc	Local
m	Meridional
pass	Passage
prop	Propulsive
r	Residence
req	Required
sys	System
t	Tip

[1] Includes only subscripts which are abbreviated or non-self-explanatory

1

Introduction

In recent years, the issue of climate change, being one of the biggest challenges of our modern societies, has gained ever-increasing levels of attention in all aspects of human activity. As such, many industries have successfully started introducing mitigating measures and new technologies at a commercially significant scale. For instance, the proportion of electric vehicles in operation is steadily increasing, which together with the continuous improvement and electrification of public transport and the expanding use of renewable energy sources is reducing the emissions of the transport sector. In the commercial aviation industry, however, no such solutions have been implemented yet. In 2018, transport aircraft were estimated to be responsible for 2.5% of the global CO_2 emissions [1], while the total effect in terms of all emitted species was determined to be closer to 3.5%. [2] As other industries continue their transition towards decarbonisation and sustainable operation, this contribution will rise to an unacceptable extent, forcing the industry to adopt one of two main options: 1. the usage of sustainable aviation fuels (SAFs) in combination with costly carbon capture (which would be required not only to reverse the direct carbon dioxide emissions, but also to balance out the non-CO_2 effects) or 2. the introduction of completely new, truly sustainable propulsion technologies, i.e. those that have no carbon emissions during operation and whose other climate warming potentials can be strongly reduced. For many different reasons, such as being more effective on a long-term perspective, the second option is favourable. Still, due to the costs associated to this and the fact that currently produced aircraft will be able to fly using SAFs for the coming decades, a mix of both options will at least initially be required.

Currently, the main technological solutions regarding the second option are 1. battery-electric and 2. fuel cell (FC) aircraft. Due to the low energy density of batteries as compared to fossil fuels, the former will for the foreseeable future only be an option for small, short-haul aircraft. [3] FCs however present an interesting opportunity for medium-range operation. They are devices which produce electricity from hydrogen and oxygen, which is then used to power electric motors that are connected to propellers. For truly sustainable operation, the hydrogen must be ”green”, i.e. it must be produced through electrolysis, using only renewable energy. Note that for the production of some types of SAFs, this hydrogen is required anyway. Using it directly in a FC would therefore prevent further energy losses. It should be mentioned that for most types of FCs, such as proton-exchange membrane (PEM) FCs, which are considered in this thesis project, water is the only exhaust emission. In general, this does potentially contribute to climate change, mainly through the formation of contrails and clouds. However, as compared to a gas turbine, this water is produced under very different conditions such as a much lower temperature, meaning that this effect can be strongly reduced. [3]

An important aspect of the introduction of any new technology in aviation is the development of sizing and design methods. These are not only required for the actual development of a commercial product, but also for research into the effect of this technology on the aircraft in general. This is especially relevant with regard to the conceptual and preliminary design phases. The current state of research into these methods for FC propulsion systems is still in its infancy, especially when compared with equivalent methods for conventional aircraft. Two particular shortcomings can be found, as will be explained later. The goal of this thesis is to attempt to fill these research gaps by proposing a new

set of preliminary sizing methods for PEMFC propulsion systems. Examples of possible applications of these methods will be demonstrated as well.

The main purpose of this report is to inform the reader about all the work that was done during the thesis project. The focus in the chapters below is mostly on the development of the methods and on the results obtained, with only a short overview of the relevant literature. The latter was presented more in detail in the previous report, at the end of the literature study phase. [4] In general, it is assumed that the reader is knowledgeable about topics such as aircraft design & propulsion and aerospace engineering in general, but not yet about FC systems. Therefore, an introduction into PEMFCs in general as well as FC aircraft propulsion systems is given as well. Furthermore, the goal of this report is not just to present the work that was done, but also to show the value of the improved set of methods that are presented, in terms of the sizing results and sensitivity studies that can be produced.

The structure of this report is as follows: this introduction is followed by chapter 2, which contains basic theory about PEMFCs and FC propulsion systems, as well as a short summary of the relevant research and a more detailed description of the research goals. In chapter 3, the overall sizing approach is explained, along with a detailed consideration of each subsystem model and the integration into the Initiator, which is an aircraft sizing environment. Next, the results are presented in chapter 4. This consists mainly of an aircraft sizing study and several sensitivity studies. Finally, a number of conclusions and recommendations for future work are listed and explained in chapter 5. This is followed by Appendix A, which contains additional results for the aircraft sizing study which are not explicitly analysed in chapter 4 but might nonetheless be interesting to consider. The code developed for this thesis project is not given in an appendix due to its length, but can be found in a GitHub repository located at `https://github.com/danieljuschus/pemfc-aircraft-sizing`.

2

Background Information & Research Goals

This chapter provides background information on the topic of this thesis in the form of relevant theory and existing literature. It starts with a description of fuel cell (FC) propulsion systems in section 2.1, followed by a short summary of the current state of FC aircraft design in section 2.2. Furthermore, the research goals and objectives are also presented in section 2.3.

2.1. General Characteristics, Functioning and Layout of Fuel Cell (FC) Propulsion Systems

This section contains a short summary of the basic characteristics FC systems, starting with the overall layout in subsection 2.1.1. The following two subsections zoom in on the cell and stack and their supporting systems, i.e. the balance of plant (BOP).

2.1.1. Layout of a FC Propulsion System

In a FC aircraft, a FC system provides electrical power to electric motors, which then transform it into propulsive power through propellers or other thrust devices. Such a system consists of a FC stack, where the main electrochemical reaction between hydrogen from a tank and oxygen from the air takes place, and additional components which support this reaction. The latter are collectively called the balance of plant (BOP). A typical layout for such a system, as applied in this thesis project, is shown in Figure 2.1. Here, the stack is supported by a heat exchanger, i.e. a cooling system, as well as a humidifier and a centrifugal compressor. Each of these parts is described more in detail in the subsections below. In most cases, it is beneficial to also include a battery as a separate energy source, effectively resulting in a hybrid system. The main reason for this is the low power density of FCs, which would lead to a prohibitively large empty mass if they were sized for the maximum power required. Instead, the battery covers such power requirements, for instance during take-off, whereas the FC only is active during cruise. Furthermore, a battery is also able to respond more quickly to any sudden changes in the power requirement. Still, the main energy source for such an aircraft is the hydrogen, which is stored in a tank. Due to the low volumetric energy density in its gaseous form, the hydrogen should be stored in its liquid state onboard of a large aircraft.

Figure 2.1 shows the conceptual layout of the propulsion system but does not yet give an indication on how this is actually placed on the aircraft. Many options exist here: most of the system components can either be placed a single time on the fuselage or can be distributed along the wing or the outside of the fuselage. For the purpose of this thesis, the focus is on complete ”FC engines” which contain every part of the FC system, as well as the electric motor (EM) and propeller. This is illustrated schematically in Figure 2.2. Multiple of these are then placed on or under the wing, or possibly on the fuselage. This presents several advantages, such as increased redundancy, easier access for maintenance and the similarity to currently used gas turbine engines. One potential disadvantage is the effect on both the

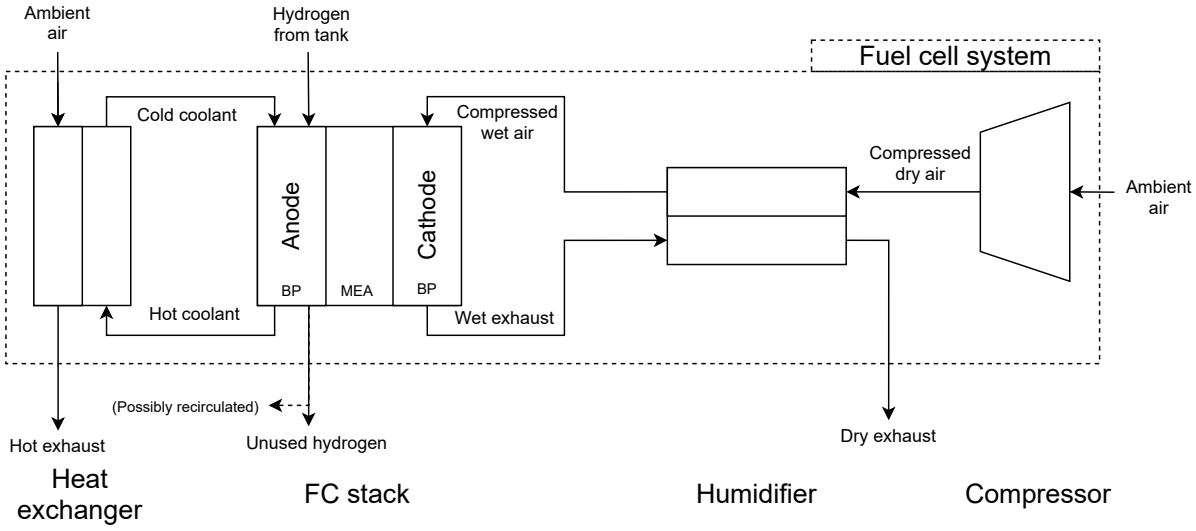

Figure 2.1: Layout of the FC system as considered in this thesis, in terms of the main gas flows, which are indicated with arrows. The coolant pump is not shown as it is mostly neglected in the modelling process (further explained in subsection 3.3.2). The stack produces the electric current, which is then consumed by the electric motors (and any other systems, in this case, the compressor). Note that the option of recirculating the anode exhaust is shown, as not all of the hydrogen is used. This would however require yet another BOP component.

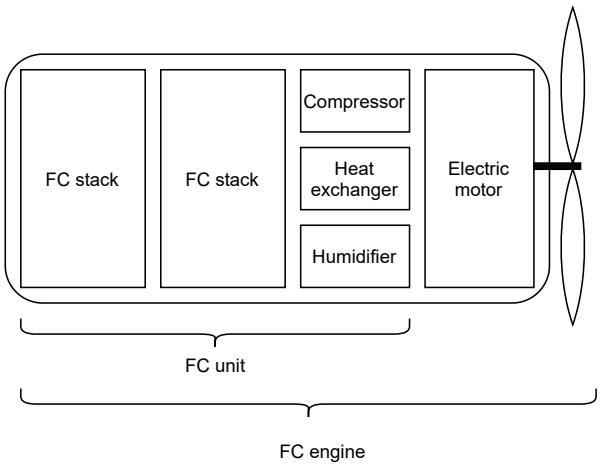

Figure 2.2: Schematic drawing of a FC engine. In this case, two stacks are present.

aerodynamics and the structural design of the wing. Within the FC engine, there can be multiple stacks in series, for reasons further explained below. In any case, there is only one set of BOP components. To clearly denote such a set of FC system components, the term ”FC unit” is introduced as well in Figure 2.2. In general, the hydrogen tank will be placed in the fuselage, in front or behind the passenger cabin. The battery, being more flexible in its shape, could be placed in the fuselage or in the wings. Note that the methods developed in this thesis would also allow other layouts if modified. To restrict the number of user inputs, the restriction to FC engines as described here is made.

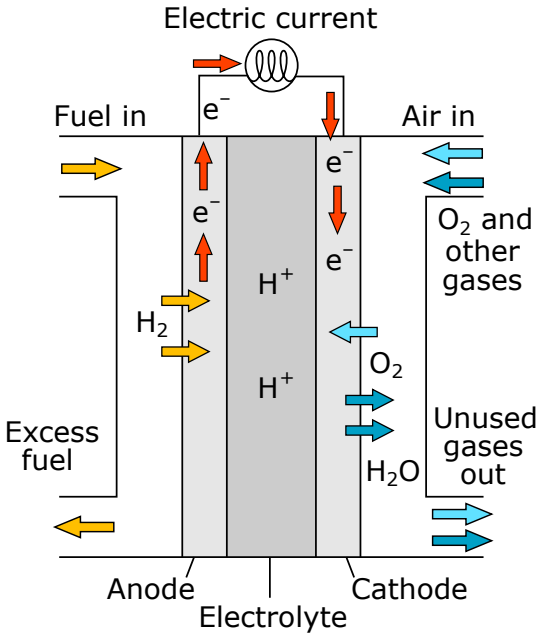

Figure 2.3: Schematic drawing of a PEM fuel cell.
Image from public domain.

2.1.2. Functioning of Proton-Exchange Membrane Fuel Cells (PEMFCs)

In any type of FC, an electrochemical reaction takes place, due to which some of the chemical energy contained in the reactants is converted to an electric current. Most often, the reactants are hydrogen and oxygen:

$$\mathrm{H_2} + \frac{1}{2}\,\mathrm{O_2} \longrightarrow \mathrm{H_2O} \tag{2.1}$$

Whereas the hydrogen comes from a tank onboard the aircraft, the oxygen is simply taken from the ambient air. The only other products of this reaction are heat and water vapour. In Figure 2.3, a schematic drawing of a proton-exchange membrane is shown. There are two electrodes: the anode and the cathode. The hydrogen enters at the anode and the oxygen at the cathode. In a proton-exchange membrane (PEM) FC, the hydrogen is split into an H^+-ion (i.e. a proton) and an electron:

$$\mathrm{H_2} \longrightarrow 2\,\mathrm{H^+} + 2\,\mathrm{e^-} \tag{2.2}$$

The former travels through the membrane, explaining the name of this FC type, The electron on the other hand causes the electric current in the external circuit. At the cathode, both are combined with the oxygen to form water:

$$\frac{1}{2}\,\mathrm{O_2} + 2\,\mathrm{H^+} + 2\,\mathrm{e^-} \longrightarrow \mathrm{H_2O} \tag{2.3}$$

One such cell produces a current in the order of magnitude of 1 V, meaning that for virtually any application, multiple cells are combined in series to form a stack, as shown in Figure 2.4, such that their voltages add up. The voltage is produced with a certain current density, i.e. an amount of current produced per unit area of the cell, which is typically in the order of magnitude of 10000 A/m^2. Multiplying these two parameters leads to a power density (W/m^2). Given a total desired output power of the cell and knowing the number of cells, the area required for each cell can be determined.

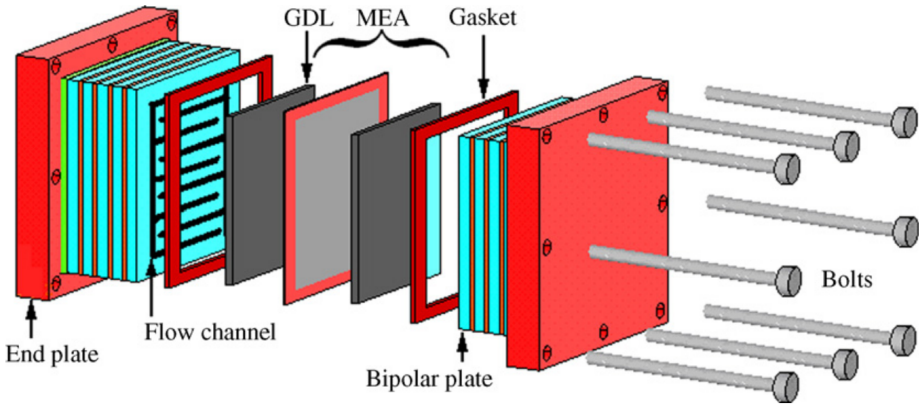

Figure 2.4: Exploded view of a PEMFC stack. [5]. In this case, assuming a typical cell voltage, the total voltage is around 8 V. Reprinted from [5] with permission from Elsevier.

In Figure 2.4, the single cell from Figure 2.3 is equivalent to the membrane-electrode assembly (MEA). Between the cells are the bipolar plates (BPs), whose main task is the delivery of the reactants through the gas diffusion layer (GDL) to the reaction sites. For this purpose, they have a network of flow channels. Their name can be explained by the fact that on one side, they provide gasses to the anode and on the other to the cathode. Other tasks of the BP include transporting the electrons from one cell to another, thereby creating the complete electric circuit through the stack, and transporting a liquid coolant. Another minor component is the gasket, which prevents any leakages. The MEA, GDL, BP and gasket together are called the repeating hardware. The non-repeating hardware such as the endplates (EPs) and the bolts sits at the end of the stack and its main function is to exert sufficient mechanical pressure on the cells.

If the desired output voltage of the system is in the order of magnitude of several hundred volts, it might be necessary to split it up into multiple stacks, as shown in Figure 2.2. The main reason for this is the difficulty of ensuring the structural integrity and an equal distribution of the mechanical pressure as the number of cells approaches 1000. Another option would be to include a voltage converter. This would come with additional penalties and is not considered in this thesis to simplify the modelling. It would on the other hand prevent the mass penalty associated to the doubling of some of the non-repeating hardware.

Although many other types of fuel cells exist, the PEM type is chosen for this research project. One of the main reasons is the high technical readiness level (TRL), having been applied on a commercial level in other types of transport such as automobiles and trains. This large amount of experience is one of the reasons why they can be designed in a compact and lightweight way. Although stacks with higher operating temperatures have been demonstrated at lower TRLs, so-called LT-PEMFCs (low temperature), which are considered in this thesis, operate significantly below the boiling point of water. On one hand this means that they start up quickly, which is important for most transport applications. On the other hand, this also means that the rejected heat is at a much lower temperature than for example that of a gas turbine. Not only does this make any potential heat recuperation difficult, it also requires large heat exchangers due to the low temperature difference with the ambient air. This is contrast with other types such as solid oxide FCs (SOFCs), which operate at up to 1000°C. Although they are less common in transport applications, this type has also been proposed for aircraft propulsion systems. This would however significantly change the BOP in many ways, as well as requiring many changes in the stack and cell models. Therefore, this thesis specifically specialises in PEMFCs. Other noteworthy disadvantages of the latter include the expensive materials contained in the stack (such as platinum) and the required purity of the hydrogen.

2.1.3. Role and Functioning of the Most Common Balance of Plant (BOP) Components

Figure 2.1 shows the three main BOP subsystems that are likely required for a transport application of the size and with the operating conditions of an aircraft: the compressor, the heat exchanger and the humidifier.

The Compressor

The role of the first component, the compressor, is to increase the pressure of the cathode inlet air. As will be explained further in the modelling chapter, the efficiency of a FC decreases with the reactant pressure. Whereas the hydrogen is pressurised in the tank, the ambient air is at a significantly lower pressure at the cruise altitude. A compressor can therefore help to limit the losses associated to the operation at high altitude. [6] Note that currently, there is still a lack of experience with the operation of FCs at high altitude, meaning that a manufacturer will most likely require the stack to be operated at or near sea-level pressure. This would however result in a very large compressor. The choice of the compression ratio is therefore highly important for the design of the entire aircraft. Note that the flight speed does result in a certain amount of pre-compression in the inlet of the compressor, as the freestream slows down. The most suitable type for this application is a centrifugal compressor, mainly due to its compact size and low weight. [7, 8] Although it would be possible to drive the compressor with the exhaust gasses, here it is driven by an electric motor, to simplify the modelling. The power is in that case provided by the stack.

The Heat Exchanger

A PEMFC typically has an efficiency of up to 50%, which means that the amount of heat produced is of the same order as the electric power output, presenting a considerable heat rejection requirement for larger vehicles. [9] Liquid cooling is often seen as the most suitable option as it offers the best performance. [10] This comes at the cost of system complexity, as compared to e.g. air cooling. Also, a large heat exchanger is required due to the low temperature difference between the coolant and the ambient air. [10] A liquid cooling system usually consists of the liquid coolant, a coolant pump and a heat exchanger (HX). The coolant is heated up in the bipolar plates of the stack and rejects its heat to the ambient air in the HX. [11] Modelling-wise, the HX and the liquid coolant will be accounted for, in terms of their mass. As will be explained later, the drag of the HX will be, in this first study, ignored.

The Humidifier

The third BOP component considered here is the humidifier. While water is constantly produced at the cathode, it is also removed through various mechanisms, such as simply being blown out with the exhaust gas. During the operation at high current densities (as will be the case during cruise), the rate of water rejection is higher than the production rate. [12] This means that without a humidification system, the membrane would dry out, which would prevent the transport of the protons, as well as damaging the cell. [13] For a large system such as an aircraft propulsion system, external humidification is most likely needed due to the size of the stacks. [14] In this case, additional BOP components are required, as opposed to internal humidification. A popular option is the use of a membrane-based gas-to-gas humidifier, where the humidity present in the cathode exhaust is partially transferred to its inlet. [12] This is done in an external component, which sits between the compressor and the stack. As will be explained later, there are many small channels in which the opposing flows are separated by a membrane, through which the humidity is transferred. [12] Compared to other types of external systems, such a humidifier suffers from less parasitic losses and is simpler by design. [12]

2.2. Design of Fuel Cell Aircraft

Fuel cells are not a new technology, having first been described around 180 years ago. Since then, they have been applied at a commercial scale not only in stationary applications, but also in various large vehicles such as busses or trains. However, regarding the aviation industry, only unmanned or small manned prototypes, such as the DLR HY4, have achieved flight. Although several FC transport

aircraft are in the early stages of development at the time of writing, no CS-25 aircraft has flown being fully powered by FCs. An important part in the implementation process of this technology in the industry will be the development of design & sizing methods. For gas turbine systems, a wide range of methodologies with different levels of detail has been developed over the last decades.

One of the most important tasks during the design of an aircraft is the determination of its mass at various points along its missions. During the conceptual design phase, this is only done at the level of the complete aircraft, i.e. determining values such as the maximum take-off mass (MTOM) or operational empty mass (OEM). In the subsequent preliminary phase, the various systems that make up the airframe are considered separately. While in early stages, this is often done with single-equation statistical Class 2 relations, more detailed Class 2.5 or 3 methods are later applied. With an increasing level of detail, the mass estimation also becomes more and more entangled with the performance analysis.

Looking at the limited amount of existing literature on the design of FC aircraft, one will notice that usually, much more effort is put into the performance estimation, while the mass of the FC system is only addressed at a very basic level. In many studies of FC-powered UAVs, existing off-the-shelf FC systems are taken as an input to the sizing process, removing the need for a weight estimation method [15, 16] In some cases, the authors go a step further by deriving statistical relations from the weight of such systems, for instance w.r.t. the output power [17]. This approach is not suitable for larger aircraft, as no stacks of a corresponding power are directly available and because it severely restricts the iterational character of the process. Regarding larger transport aircraft, a popular approach for the estimation of the FC system mass is the usage a fixed value for the specific power of the system. This metric indicates how many watts the system can produce per kilogram of mass. Often, it is just roughly based on previous experience or general trends. [18, 19] A 2018 paper by Kadyk et al. [20] shows a particularly clear example of the commonly found contrast between the mass and the performance estimation: while for the former, only a single value for the constant specific power is used, the core of the latter consists of a very detailed, multi-equation analytical voltage model. Similar models that address the mass of all components of the system seem to not yet be available in open literature. [21]

The main issue with the mass estimation approaches described above is that the power required and the operating conditions encountered by a transport aircraft will be very different from those that current off-the-shelf FC systems for transportations are designed for. Furthermore, the designer lacks the ability to analyse the influence of various parameters, such as the atmospheric conditions, on the resulting mass. It should also be noted that nearly all existing literature concerns specific design studies or the analysis of a certain parameter, rather than attempting the development of general methodologies. The only such work that could be found during the literature study was done in a 2017 Master thesis by Comincini. [22]

It is interesting to shortly mention possible reasons for this research gap. In all current applications of FCs, for instance in busses, the mass of the propulsion system is much less critical as compared to an aircraft. Of particular interest are for instance the cost of the system, or its volume. For an aircraft on the other hand, the empty mass is a crucial parameter, which directly influences the fuel usage. Moreover, current systems, both stationary and in vehicles, operate at or near the sea level. This means that in terms of the temperature and the pressure, both the absolute value and the range of nominal operating conditions is very different for an aircraft. This requires different design solutions at the level of the complete propulsion system and can also have an additional effect on the mass, which could not be resolved otherwise.

2.3. Research Goals

As explained in the previous section, there is currently a research gap in the design of FC aircraft: there is a lack of design & sizing methods that properly address the mass of the propulsion system components during the preliminary design phase, especially as compared to the determination of the performance. Developing such methods would have a significant positive impact on the accuracy of the design, especially since FC systems have a much lower specific power than gas turbines. Additionally,

research has shown that the feasibility of a given conceptual design can be highly dependent on the exact value of the specific power. [23] Therefore, the objective of this research project is **to develop PEM fuel cell propulsion system sizing and analysis methods for the preliminary aircraft design phase in order to more accurately address the weight estimation of this system.**

Connected to this are the main research questions, as determined during the literature study phase [4]:

1. How can the accuracy of the weight estimation of PEMFC propulsion systems during the preliminary design phase of an aircraft be improved?
2. How sensitive is the weight of a PEMFC propulsion system w.r.t. various aircraft sizing inputs?
3. How does the weight of a FC transport aircraft compare to that of a corresponding kerosene powered one?

As no FC transport aircraft exist yet, it will be necessary to rely on physics instead of statistics. In this case, it is important to realise that the mass of the propulsion system cannot be estimated in isolation of its performance. This means that a complete propulsion system model will be developed. Where possible, existing methods, especially for the performance aspects, will be applied. The development and validation of the propulsion system model will address the first research question. For the remaining two questions, it will also be necessary to implement this model in an aircraft sizing environment. This will allow sensitivity & design studies to be performed on the level of the complete aircraft. This will not only demonstrate the capabilities of the new modelling approach, but will also allow more general statements about the characteristics and behaviour of FC aircraft to be made, which will further underline the value of this research project.

Several requirements will have to be met by the model. Firstly, it should be modular, to allow the integration of different propulsion system elements or of the current elements in a different layout. Initially, the focus will be on the layout presented previously in this chapter. In later stages however, it should be possible to easily replace or add different technologies or components without having to change the rest of the program. Secondly, the model should be parametrised, to facilitate the integration within an aircraft design environment. This means, amongst others, that there should be a clear definition of all input and output parameters. Thirdly, it should be scalable, to allow the application to any CS-25 aircraft. This will require the applied methods to be general enough, without losing too much accuracy. Fourthly, all constants should be chosen such that the results correspond to the current level of technology of FC systems. Finally, attention should be paid to limiting the computational time required, again to make it more usable in an iterational aircraft design process.

At this point, it is interesting to note that there are several aspects which will facilitate the development of this model. Firstly, a fuel cell stack has no moving parts and is therefore mechanically and geometrically simpler than a modern gas turbine, which can have many turbomachinery stages and multiple spools. A PEMFC stack is also simpler to model from an aerodynamic and thermodynamic perspective, as it operates at low temperatures and without any high internal velocities. One of the consequences of this is that a stack is highly scalable. In principle, an increase in power will just result in an increased area per cell. In comparison, gas turbines suffer from severe scaling effects such as those due to the Reynolds number. In terms of the BOP, the compressor is the only component with major moving parts, meaning that its modelling will be the most complex. Finally, as mentioned before, PEMFCs have reached a high level of technical maturity, meaning that despite the lack of commercial implementation in the aviation industry, there is a large amount of knowledge available.

3

Methodology

Following the previous derivation of a research goal, this present chapter describes the development of the propulsion system model. After a description of the overall sizing approach in section 3.1, the modelling of the stack and the BOP are presented in section 3.2 and section 3.3 respectively. Next, the integration of the propulsion system model into an existing aircraft sizing environment is described in section 3.4. Finally, section 3.5 contains a summary of the limited validation activities that could be performed in this project.

3.1. Overall Fuel Cell System Sizing Approach

The overall approach for the FC system sizing process is shown in Figure 3.1. The starting point is the cell model, which provides a cell voltage V_c, as well as a cell efficiency η_c. Next, an internal iterational loop is run. At the first iteration, the stack only needs to produce the propulsive power P_{prop} (i.e. the electrical output power of the complete system, which will be used for propulsion). Having run the compressor performance model for the first time, a first value for the power required P_{BOP} is known, which is added to P_{prop} to obtain the total power that the stack needs to produce. This continues until the compressor reaches convergence. Note that this is the only BOP component that is assumed to consume power in this case. If more detailed models are implemented in the future, for instance for the coolant pump, more components will have to be added to this loop. After this, the compressor mass model, the other BOP models and the stack model are run. For the stack model, another important input is the system voltage. This means that there are two main performance inputs (propulsive power P_{prop} and system voltage V_c) and two outputs (efficiency η_{sys} and mass of the complete system m_{FCunit}).

Note that the drag is not considered anywhere in this approach. Each of the components contribute to an overall increase in drag, not only through their mass, but also due to various internal losses and external parasitic drag components. However, as the focus of this thesis is on the mass and the performance of the system itself, this not yet included. Drag estimation at this level of detail is in general difficult, but could be done by considering the frontal and wetted areas of the FC engines. These in turn result from the dimensions of the various subsystems (which are already a by-product) and their layout. This should be implemented in the next version of the model. It should also be mentioned that this process is implemented as a Python 3.9 script, calling separate functions containing each submodel. The code for this script as well as all functions can be found in a GitHub repository located at `https://github.com/danieljuschus/pemfc-aircraft-sizing`.

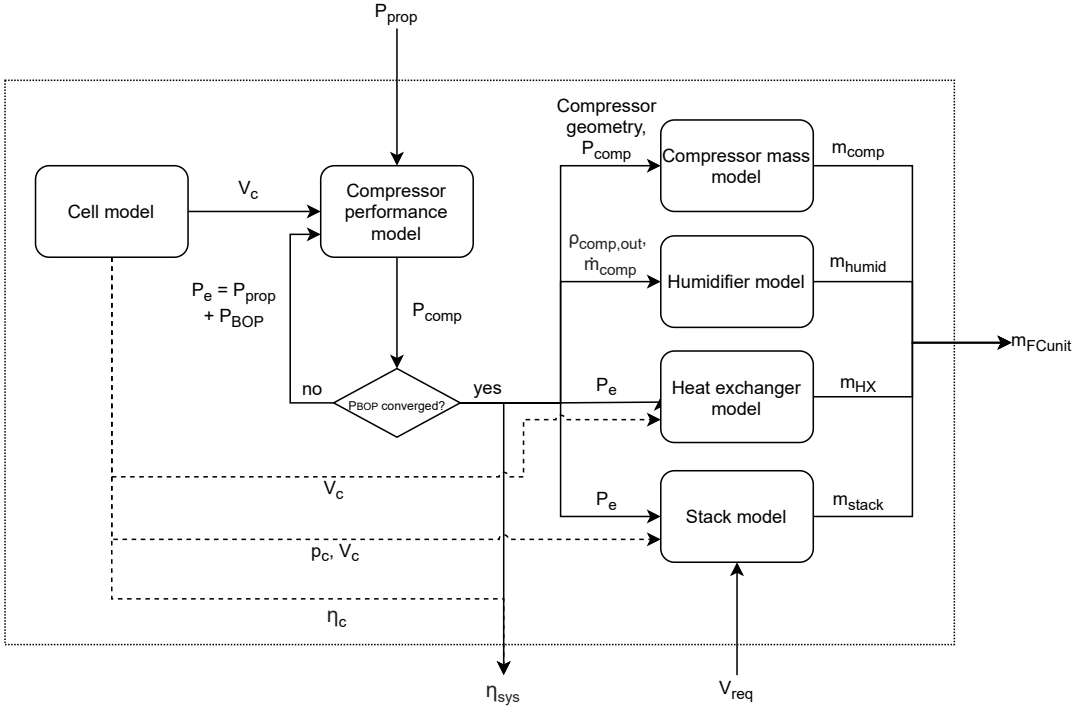

Figure 3.1: Diagram showing the FC system sizing approach used in this thesis. The unbroken arrows show the flow of the sizing process. The broken arrows only indicate the flow of additional variables.

3.2. PEMFC Stack Modelling

This section contains a description of the stack performance modelling in subsection 3.2.1 and the mass modelling in subsection 3.2.2.

3.2.1. Stack Performance Modelling

The basis of any FC performance model is a so-called polarization model. It expresses the cell voltage V_c as a function of the current density j, often in the form of a single equation, as shown in Equation 3.1. This can be found in different forms in many textbooks. In this case, the notation presented by O'Hayre et al. [24] is mostly followed. The first part of the equation is E_0, which is the reversible electric potential of the hydrogen-oxygen reaction at standard-state, as determined from the corresponding Gibbs free energy. It is equal to 1.229 V. Next are the deviations from this ideal value due to non-standard conditions, i.e. a certain temperature T and reactant pressures p. R is the gas constant and F the Faraday constant. The last part of the polarization model are the deviations due to voltage losses, which itself consists of three different loss mechanisms. The first one is the activation loss, which describes the reduction of the voltage that is necessary especially at low current densities to overcome the kinetic energy barrier at the electrodes. It depends on two constants, the transfer coefficient α and the exchange current density j_0. It is usually only accounted for at the cathode. Next are the combined ohmic losses which occur in any electric circuit. Those are often expressed with a constant r. The last major loss mechanism is the mass transport loss, which arises from the difficulty of enough reactant molecules reaching the reaction sites at high current densities. It depends again on a constant c and on the limiting current density j_{lim}, at which this loss causes the voltage to drop to zero. Note that there is another term j_{leak}, the leakage current density, which accounts for any leakage of reactants or other parasitic losses occurring during the reaction.

$$V_c(j) = E_0 - \underbrace{\frac{\Delta s}{2F}(T - T_0) + \frac{RT}{2F}\ln\left(p_{H_2}\sqrt{p_{O_2}}\right)}_{\text{Deviation due to non-standard conditions}} - \underbrace{\frac{RT}{2\alpha F}\ln\frac{j + j_{leak}}{j_0} - rj - c\ln\frac{j_{lim}}{j_{lim} - j - j_{leak}}}_{\text{Deviation due to losses}} \quad [V] \tag{3.1}$$

Table 3.1: Values of the constants in the polarization model used in this thesis. Based on the value proposed by O'Hayre et al. [24], with minor modifications.

Transfer coefficient at the cathode α	Area specific resistance r	Mass transport loss constant c	Limiting current density j_{lim}	Leakage current density j_{leak}
0.3	$10^{-6}\ \Omega m^2$	0.5 V	20000 A/m^2	100 A/m^2

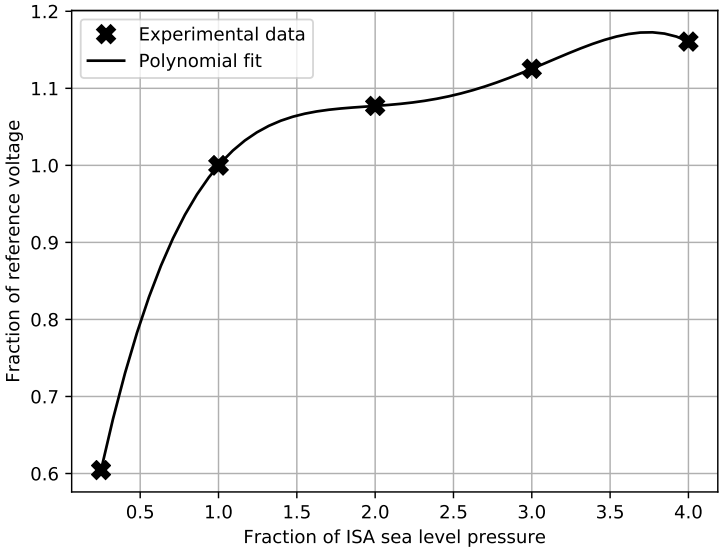

Figure 3.2: Basic voltage loss model for operation at non-sea-level ambient pressure, derived from two sources of experimental data. [6, 26]

The efficiency of the cell η_c is simply the fraction of the cell voltage over the value of 1.482 V, as shown in Equation 3.2. [25] The latter is the voltage that would be obtained if all the chemical energy from the reaction was converted to a current. It results from the enthalpy values (instead of the Gibbs free energy). Note that for a PEMFC, the higher heating value (HHV) is used, as the resulting water is liquid. The efficiency of the complete system η_{sys} contains two more elements. Firstly, the fuel utilisation factor μ_f added. [25] As indicated in Figure 2.3, not all the hydrogen is used at the cathode. A good first approximation for this value is 0.95. [25] Note that this also means that no hydrogen recuperation takes place. Secondly, the additional power consumed internally needs to be accounted for by the fraction of the propulsive output power P_{prop} over the stack output power P_{stack}. This means that η_{sys} in this case is the efficiency in terms of the incoming fuel power and the outgoing electrical power. This definition is needed for the aircraft sizing, as explained later in section 3.4.

$$\eta_{sys} = \eta_c \mu_f \frac{P_{prop}}{P_{stack}} = \frac{V_c}{1.482} \mu_f \frac{P_{prop}}{P_{stack}} \tag{3.2}$$

Table 3.1 shows the values of all constants as used in this project. Some have been shown to be a function of the operating conditions. However, no suitable analytical model has been described in open literature to account for this. Therefore, as explained in the next section, the BOP will be sized by default such that the stack receives sea-level pressure. Still, for some sensitivity studies, it will be interesting to at least gain some idea of how the pressure will influence the losses. For this purpose, a simple model was derived from two existing experimental studies. [6, 26] A polynomial fit was performed on experimental data of fuel cells operating at different altitude, as shown in Figure 3.2.

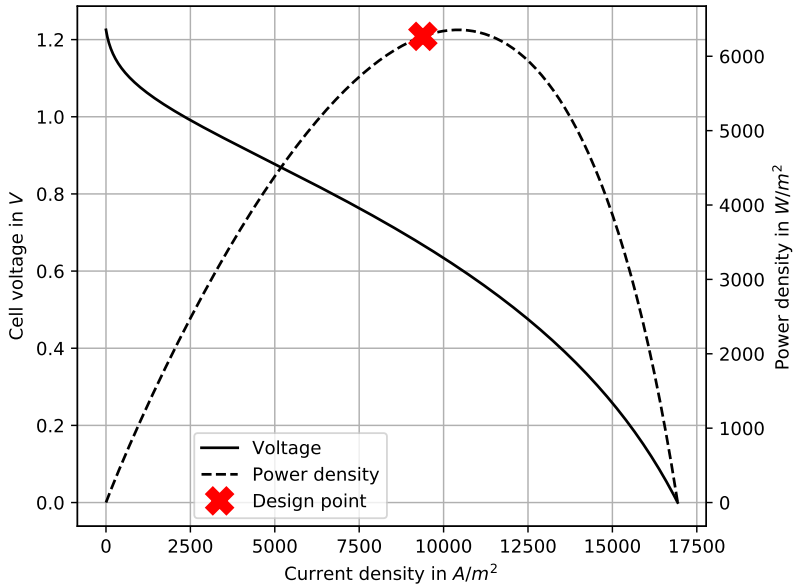

Figure 3.3: Voltage and power density curves resulting from the polarization model. The design point for the default oversizing factor of 10% is shown. Note that negative voltages at high current densities are cut off.

Applying Equation 3.1 leads to the polarization curve in Figure 3.3. Multiplying the voltage with the current density leads to the power density p_c, the second line shown in this figure. Also shown is the design point, or the nominal operating condition of the cell at continuous power. At first, one might be tempted to place this at the peak of the power density curve. However, with higher current densities, the efficiency of the cell continuously decreases, as can be seen in Figure 3.3. Therefore, an operating point at the left of the peak results in a higher efficiency, at the cost of a lower power density. From the perspective of the entire aircraft, the former will result in a lower fuel mass as well as lighter BOP components (due to less air being required and less heat being produced, as explained later), whereas the latter will result in a heavier stack (as the stack area will have to be increased to maintain the same power). This offset from the peak power density is expressed with the so-called cell oversizing factor. [20] Unless mentioned otherwise, this factor is kept at 10%, which is also the value shown in the figure. Choosing the value of this factor as a design input will therefore present a trade-off between various masses.

Everything described in this subsection up to this point is contained in the cell model of Figure 3.1. A few more performance related calculations are done in the stack model. Firstly, the number of cells in the stack is equal to the required output voltage divided by the cell voltage. Today, stacks with cell numbers in the low hundreds can be found. However, if the voltage approaches 1 kV, as can for instance be seen with the newest generation of electric vehicles, the structural integrity of the stack becomes an issue. In that case, it is advisable to split up the single stack into multiple ones, as already briefly mentioned in subsection 2.1.1. The last parameter that remains for a complete description of the stack is total cell area. This is equal to the required stack power (i.e. the required propulsive power plus the compressor power) divided by the power density at the design point of the cell.

3.2.2. Stack Mass Modelling

The mass estimation of the stack is done in the stack model of Figure 3.1, after having determined all performance parameters. The stack is broken down into its main components, as described in subsection 2.1.2. The contribution of the gaskets is assumed to be negligible. For the MEA, an area density of 0.2 kg/m^2 is assumed. [20] For all other components, 304L stainless steel is assumed as the material, which has a density of 8000 kg/m^3. This is a common choice for components such as the bipolar plates. [27] Based on previous research [28–30], thicknesses of 0.2 mm and 25 mm are assumed for the bipolar plates and the endplates, respectively. Knowing the number of cells and the area per cell,

the mass of these components follows. The determination of the bolt mass is slightly more complex. Theoretically, it should be possible to perform a simple structural sizing of the bolts if the mechanical pressure to be exerted on the stack is known. However, it is difficult to find a conclusive way to determine this pressure in open literature. Therefore, the diameter is instead determined as a fraction of the side length of the cell, assuming a square shape. This is based on existing designs for which this value could be obtained. Furthermore, it has been shown in some cases that 10 is an ideal number of bolts. [31]

Now the total mass of the stack is obtained, as also shown in Equation 3.3. Note that the dimensions of the stack are a by-product of this procedure, as all thicknesses are known. Although this is not done in this thesis, the dimensions could be used for a more detailed layout of the system and a subsequent drag estimation based on the frontal or wetted area of the engine. Although similar approaches have been shown in literature, the constants are often just based on previous experience or rough guesses instead of being supported by corresponding research.

$$m_{stack} = A_{cell}\left[n_{cells}(t_{BP}\rho_{BP} + \rho_{MEA}) + 2t_{EP}\rho_{EP}\right] + n_{bolts}\pi\frac{{D_{bolt}}^2}{4}l_{bolt}\rho_{bolt} \qquad [kg] \tag{3.3}$$

3.3. Balance of Plant Modelling

As shown in Figure 3.1, each of the three BOP components considered in this thesis is included as a separate model. In the following subsections, each model is presented. It is worth mentioning that in general, the focus was put on the compressor model, resulting in a more detailed approach, as compared to the other subsystems. This is not only because it can be expected to be the heaviest component of the FC system, but also because it consumes significant additional power, meaning that it eventually influences the MTOM of the aircraft in multiple ways. Furthermore, if the compressor ratio is chosen such that the stack receives sea-level pressure, its design is directly affected by one of the main characteristics of an aircraft: the high cruise altitude. Likewise, if the compressor ratio is chosen more freely, the output pressure has a direct influence on the stack.

It is also interesting to note that out of the three BOP subsystems, the compressor is the only component which is currently commercially available in this form and from many companies. While e.g. a specific FC heat exchanger is hard to find, there are several options for electrically-driven centrifugal compressors for the specific application in a FC system. One might be tempted to therefore resort to a statistical model for the determination of the mass of this component, for instance by expressing it as a function of the compression ratio, mass flow of air or power required. However, this would make the overall model less sensitive to various design inputs. Also, the available compressors are much smaller than what would be needed for a large aircraft. Especially given the intention to focus on the compressor, a physics-based model was therefore developed, just like for the other subsystems.

The final remark to be made before zooming in on the different subsystem models is that in each case, an existing sizing approach is replicated in a simplified way. Instead of constantly repeating the citations throughout the subsections, it will be made clear which simplifications were introduced by the author of this thesis. This means that the rest of the methodology presented is taken from the reference work. Furthermore, not every single detail of each method will be explained. Instead, just the main steps will be presented. To learn more, the reader is invited to consult the Python code belonging to this thesis, as well as the original references.

3.3.1. Modelling of the Electrically Driven Centrifugal Compressor

The compressor model implemented here consists of a simplified version of a complete sizing process as proposed by Gambini & Vellini [32] and shown in Figure 3.4. Given a number of inputs, the kinematics are first resolved, followed by a consideration of the thermodynamics and the geometrical design. This results in a required power and a mass as the main outputs. The first set of inputs are related to the performance. They are the compression ratio β coming from the main FC system sizing script, the aerodynamic inlet conditions and the mass flow of air $\dot{m}$. The latter is given by Equation 3.4, where M_{air} is the molar mass of air, P the power to be produced by the stack and λ the stoichiometric ratio

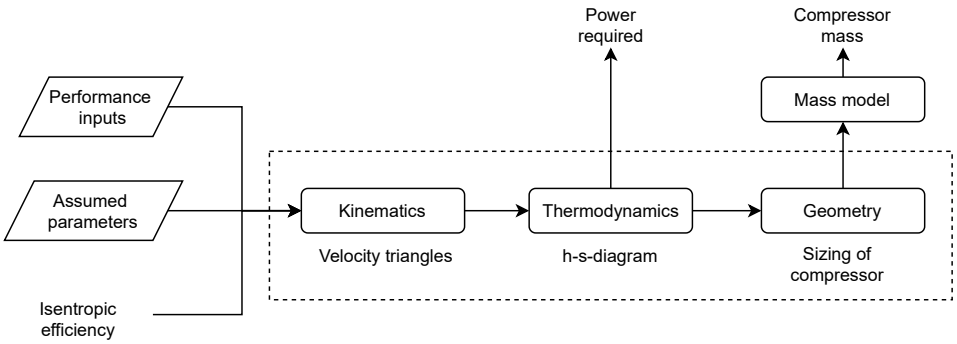

Figure 3.4: Flow diagram of the compressor sizing process. The box with the broken line indicates the extent of the original method as proposed by Gambini & Vellini [32] (excluding the loss model, which has been replaced by adding the isentropic efficiency as an input).

(for which a good approximation is 2 [25]). For the inlet conditions, it is assumed by the author of this thesis that the flow slows down completely in the inlet, such that its total conditions become the static ones. As first mentioned in subsection 3.2.1, β is chosen by default such that the stack receives the ISA sea-level pressure. This can be overwritten by the user if desired.

The next set of inputs are six parameters that are assumed to be constant and equal to a value in a typical range as determined by Gambini & Vellini. Namely, they are the work coefficient (a dimensionless parameter), two rotor diameter ratios, the rotor outlet flow angle and the inlet flow angle. This is done to prevent the necessity of solving a large system of equations. Finally, the isentropic efficiency of the compressor is an input as well. This is different to the original method and was introduced by the author of the thesis. In the original method, the efficiencies of both the rotor and the stator are determined using a number of loss relations as the last step of the process. The process is then repeated until convergence of the efficiencies is achieved. The main reason for this simplification is that no suitable loss models could be found in open literature. Most models are intended for industrial, stationary applications, which differ significantly from the type of machine required for a FC aircraft propulsion system. Instead, the isentropic efficiency is taken as 75%, which is based roughly on freely available compressor maps from companies such as Rotrex.[1]

$$\dot{m} = \frac{M_{air} P \lambda}{0.21 V_c F} \qquad \left[\frac{kg}{s}\right] \tag{3.4}$$

The first step of the sizing process is the consideration of the kinematics of the rotor. Relations between dimensionless parameters, velocities and angles are used to obtain a full description of the velocity triangles of the rotor, shown in Figure 3.5. Next, the thermodynamic parameters at each stage of the enthalpy-entropy diagram are determined, starting with the rotor inlet conditions and finishing with the total stator outlet conditions. This is first done for the isentropic processes (i.e. assuming no losses), during which the entropy stays constant. After that, the effect of the efficiency is added, leading to a different enthalpy at the same pressure. Finally, relations between the dimensions of the compressor, shown in Figure 3.6, and the other parameters determined here above are derived. For instance, the rotor diameter D_2 follows directly from the RPM and the rotor outlet blade speed u_2. At the end of the process, the applicability of the result is verified by checking whether three parameters (the divergence angle, a blade loading parameter and an area ratio) are within an expected range. If this is not the case, then the design input parameters such as the work coefficient need to be modified.

The first main output of the model, the power required to run the compressor, is simply equal to the total difference in enthalpy times the mass flow:

$$P_{comp} = \dot{m}(h_3 - h_1) \qquad [W] \tag{3.5}$$

[1] See for example `https://rotrex-fuel-cell-compressor.com/fuel-cell-compressors/`

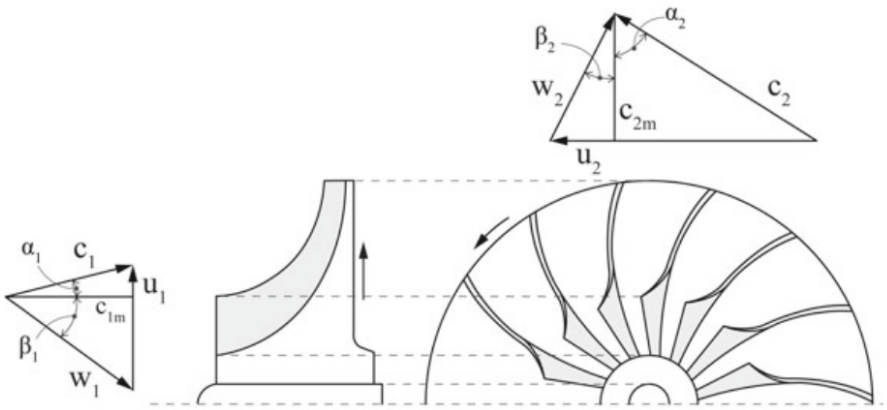

Figure 3.5: Velocity triangles at the rotor. All velocities and angles shown here are solved by the kinematics model.
Adapted by permission from Springer Nature Customer Service GmbH: [32]

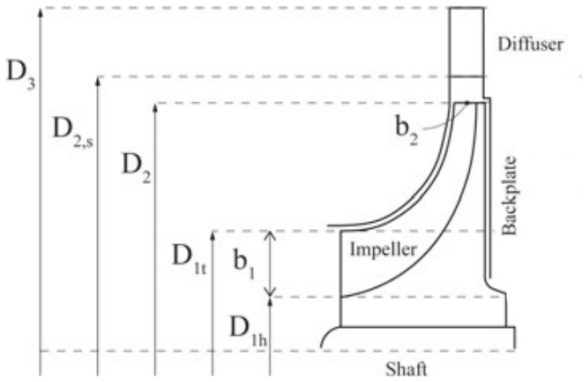

Figure 3.6: Dimension of the impeller and the surrounding geometry. Although all parameters are determined in the original method, not all are relevant for the generation of the CAD model and the subsequent mass determination. For instance, the blade heights b_1 and b_2 are not needed, as the blades are ignored.
Adapted by permission from Springer Nature Customer Service GmbH: [32]

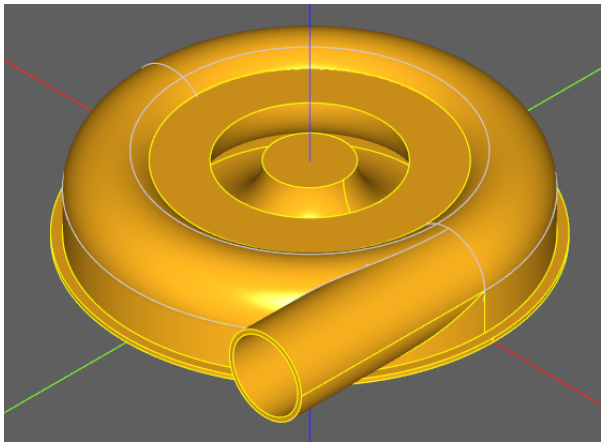

Figure 3.7: Rendering of the compressor body CAD model in Cadquery. This rendering is not created by default.

The second main output is the mass of the compressor, for which the modelling approach is not included in the original method by Gambini & Vellini. The mass consists of three parts: the compressor body, the electric motor and the bearing assembly. The compressor body in turn consists of a moving part, the impeller, around which the non-moving part, the casing, is built. Both are complex shapes for which no simple analytical formulas exist. Furthermore, the impeller design depends on many different parameters, as shown in Figure 3.6. Therefore, it was decided to obtain the mass of the compressor body from the material volume of a CAD model which is generated within the sizing process. The latter is done using the CadQuery 2 Python library. A rendering of the model is shown in Figure 3.7. For both the stator and the rotor, the blades are ignored as they only marginally contribute to the mass. [33] For dimensions that are not an output of the sizing method, such as for example the thickness of the backplate, the constant thickness is taken as a fraction of the outer diameter. This is based on reference designs for which this value was available. Similarly to the stack mass model, stainless steel is assumed as the material. The next part of the compressor mass is the electric motor, which depends mainly on the power that the motor needs to deliver. For the specific power, a current value around 2 kW/kg is assumed. This was tuned further during the validation process, which is explained later in section 3.5. Finally, the bearing assembly is taken to be a fixed fraction of the total compressor mass. This is based on a single commercial compressor produced by Celeroton, for which this value is openly available.

3.3.2. Modelling of the Plate Heat Exchanger

The sizing of the heat exchanger is based on the work by Kožulović [9], with the addition of several simplifications. The starting point is the heat rate $\dot{Q}$ to be dissipated, determined from Equation 3.6. [25] Again, P is the power produced by the stack. This heat is rejected to the air flow in a number of tubes, with the coolant flow being directed in the opposite direction, as shown in Figure 3.9. First, the expansion of the flow in the inlet of what is conceptually close to a ramjet engine (as indicated in Figure 3.8) needs to be determined. This is done by assuming various constants, such as the pressure ratio. Knowing the aerodynamic conditions at the tubes and fixing their cross-section, the heat transfer per tube $\dot{Q}_{tube}$ can be determined using Equation 3.7, where c_p is the specific heat and ΔT_{fluid} the total change of each fluid along the tube. The latter is taken as a fixed percentage of the total temperature difference between the hot coolant and the cold air. Now the required number of tubes can be simply determined. Next, the local heat transfer from the coolant through the metal to the air (with ΔT_{loc}) is considered with Equation 3.8. α_{comb} is the combined heat transfer coefficient of all media, and depends on a number of non-dimensional values such as the Reynolds number as well as an assumed thickness of the metal. A is the material surface area of a tube (not the cross-section). Now the length of the tubes can be determined, given that this is a simple function of A and that $T_{coolant,in} - T_{air,in} = \Delta T_{fluid} + \Delta T_{loc}$. At this point, a complete geometric description of the heat exchanger is obtained, leading to a mass. Note that a factor of 1.2 is applied to both the length of the tube and the total mass, to account for simplifying assumptions and the mass of the coolant pump. Also included in the subsystem mass is the coolant, which is assumed to be twice the amount that fits

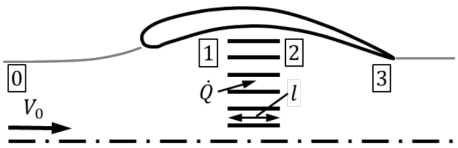

Figure 3.8: Schematic drawing, illustrating the general approach to the modelling of the heat exchanger, as proposed by [9]. v_0 is the velocity of the inflow, which flows through what is essentially a ram engine.

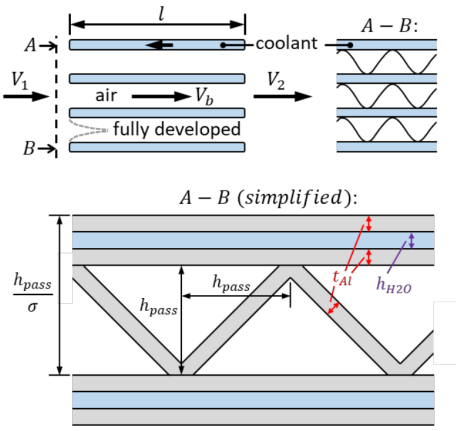

Figure 3.9: Close up drawing of the structure of the heat exchanger tubes. Both a side and a frontal view are included. [9]

in the heat exchanger. The main difference to the original method presented by Kožulović is that both the small amount of thrust produced by heating up the air flow and the parasitic drag caused by the heat exchanger in general are ignored. This is in line with the other modelling approaches in this thesis, which ignore the parasitic drag contribution.

$$\dot{Q} = P\left(\frac{1.482}{V_c \mu_f} - 1\right) \qquad [W] \tag{3.6}$$

$$\dot{Q}_{tube} = \dot{m}_{tube} c_p \Delta T_{fluid} \qquad [W] \tag{3.7}$$

$$\dot{Q}_{tube} = \alpha_{comb} A \Delta T_{loc} \qquad [W] \tag{3.8}$$

3.3.3. Modelling of the Membrane-Based Gas-to-Gas Humidifier

For the modelling of the humidifier, the method presented by Huizing et al. [12] is implemented with a number of simplifications. Figure 3.10 shows the basic layout and functioning of the humidifier, which are similar to the heat exchanger presented here above. There is a counterflow in channels that are separated by a material through which the desired quantity, in this case water, is transferred. The starting point however is different. Instead of having to determine a certain amount of humidity to be transferred per second (as is the case with the heating rate $\dot{Q}$), it is simply desired that as much water as possible can be recovered from the cathode exhaust. This is because at practical current densities, i.e. during nominal operation of the stack, the rate of water removal is in principle always above the rate of production. [12]

The first important parameter in this sizing process is the ratio R between the residence time of a moving control volume in the tube τ_r and the time τ_d for a molecule of water to diffuse through the membrane, as shown in Equation 3.9. In general, R should be bigger than 1 to allow enough water to diffuse. The second parameter is the velocity v inside the channels, given by Equation 3.10. Here, l, w and h are the length, width and height of the channels, n the total number of channels, D_W the diffusivity of water in air and Q the volumetric air flow. The latter is equal to the mass flow through the compressor divided by the air density. The dependence of the diffusivity on the temperature is ignored for the purpose of this thesis, leading to a constant value. The cross-sectional dimensions of the channels are taken as an input to the process and are based on a range of reasonable values provided by the original authors. The biggest simplification applied to the original method is that R and v are also taken as inputs to the problem, with values of 3 and 1.5 respectively, which are in the ideal ranges suggested by the authors. Instead, originally an iterational process is implemented, with various intermediate checks of several variables. Now, the system of these two equations can be solved to

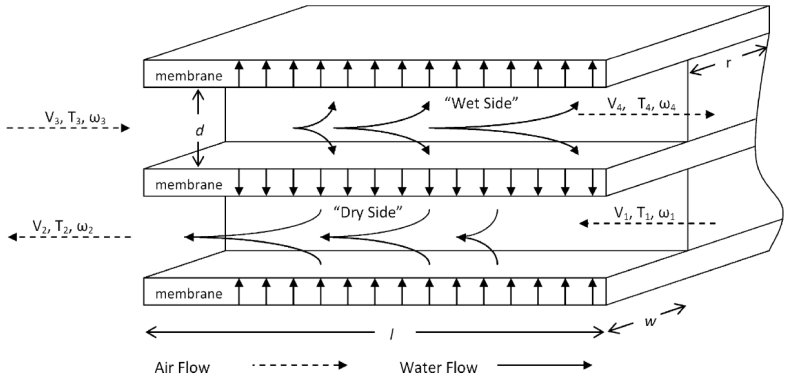

Figure 3.10: Drawing of the humidifier channels, showing the main gas flows as well as the diffusion of humidity through the membranes. [12]
Reprinted from [12] with permission from Elsevier.

obtain the length of each channel and the number of channels. This leads to a complete geometrical description of the humidifier, which together with assumptions for the materials and material thicknesses (as introduced for the purpose of this thesis) leads to the mass of this subsystem. The pressure loss through the channels is not determined here, meaning that in reality the compressor should produce a slightly higher pressure to ensure the correct value at the cathode inlet.

$$R = \frac{\tau_r}{\tau_d} = \frac{nlwD_w}{2Qh} \tag{3.9}$$

$$v = \frac{2Q}{nwh} \tag{3.10}$$

3.4. Integration of the Fuel Cell System into an Aircraft Sizing Environment

This section contains a description of how the propulsion system model was implemented in an aircraft sizing environment. As explained previously, this was done in order to perform aircraft sizing and sensitivity studies. Although this part of the research work is for the most part not specific to FCs, timewise it made up a majority of the work. Therefore, it is described in quite some detail. The section starts with a general description of the Initiator, which is the aircraft sizing tool chosen for this project, in subsection 3.4.1. This is followed by a description of the changes made to the code in subsection 3.4.2.

3.4.1. General Description of the Initiator and its Hybrid Branch

General Description of the Initiator

The Initiator is an aircraft sizing program developed in Matlab at the Faculty of Aerospace Engineering at the Delft University of Technology. Its main purpose is to obtain a preliminary design of any CS25 aircraft. The main user input is the aircraft XML input file, where the main components such as the lifting surfaces, the fuselage and the engines are defined in a very basic way, along with the design missions and a number of assumed constants such as the maximum lift coefficients. Having specified different settings in various other XML files, the sizing process can be run. At the highest level of detail, the process consists of three nested loops. The simple sizing methods that are initially used are then gradually replaced, for instance by a detailed Class 2.5 structural weight estimation of the wing. The Initiator can produce a large variety of outputs such as payload-range and power loading diagrams or a three-dimensional rendering of all main components, next to a simple numerical description of the resulting aircraft. As this suggests, it is a large, complex tool with many capabilities. Due to this, the implementation of new technologies is not a straight forward task. On the other hand, it does mean that the snowball effect caused by a different technology can be determined fully. The Initiator performs a full sizing, as well as structural and aerodynamic analysis of all main components of the aircraft in an iterational manner. This is especially valuable if, in a later iteration of the propulsion system modelling

approach of this thesis project, the parasitic drag of the FC engines is estimated properly.

One other reason for having chosen the Initiator is the support available within the Flight Performance & Propulsion department. In contrast, another option that was considered in the beginning is the aircraft design environment called SUAVE, developed at Stanford University.[2] Its advantages include being written in Python and being made specifically for the examination of novel technologies. However, next to a lack of detailed documentation and knowledge within the department, it can also not be used out-of-the-box to directly size an aircraft. Instead, the user must assemble the process from various analysis capabilities. As the main focus of this thesis is still on the propulsion system and not the aircraft sizing in general, it was finally decided to use the Initiator.

Description of the Hybrid Branch of the Initiator

Next to conventional aircraft, the Initiator is also capable of sizing hybrid-electric aircraft. Due to the differences in the sizing process, this is implemented essentially as a separate branch, meaning that several major elements of the conventional sizing process such as the mission analysis are replaced with hybrid-specific counterparts. At the beginning of the thesis project, the Initiator was capable of sizing either fully electric propulsion systems, or those that are a combination of gas turbines and batteries. Although a liquid hydrogen tank model was being developed for combustion [34], most of it could not yet be used for this thesis project due to time constraints.

The hybrid sizing methodology implemented in the Initiator is described in a 2018 paper by De Vries et al. [35] According to the nomenclature used there, a FC propulsion system is equivalent to a serial-hybrid system, of which the default layout is shown in Figure 3.11. In the case of a FC system, the gas turbine (GT) is replaced with the FC system and no gearbox (GB) or generator (EM1) are required. Note that the hybrid branch is also still able to size a conventional powertrain, which is illustrated in Figure 3.12. There, the shaft is directly connected to the primary propeller (P1). [35] This capability will be used later to verify the accuracy of the hybrid branch w.r.t. to all components that are not related to the hybrid system, by comparing the results to an existing conventional aircraft.

In general, for each component i, the sum of power paths coming out (P_{out}) needs to be equal to its efficiency η_i times the power paths coming in (P_{in}): [35]

$$\sum P_{out} = \eta_i \sum P_{in} \tag{3.11}$$

Furthermore, two power control parameters are introduced as inputs for the hybrid system: the supplied power ratio Φ and the throttle parameter ξ, which are both shown below. While the former describes the contribution of the battery to the total power from both sources, the latter describes at what percentage of its maximum power the gas turbine (or FC) is running. [35] Both most be provided by the user, for each flight phase.

$$\Phi = \frac{P_{bat}}{P_{bat} + P_f} \tag{3.12}$$

$$\xi = \frac{P_{GT}}{P_{GT,max}} \tag{3.13}$$

For the serial hybrid system, there is one additional equation, which expresses the fact that only the secondary propeller (P2) is propelling the aircraft [35]:

$$P_{p2} = P_p \tag{3.14}$$

In this way, a system of eight equations[3] is obtained for any given flight phase, such that one can solve for all power paths. [35]

[2] See `https://suave.stanford.edu/`

[3] Equation 3.12, Equation 3.14 and one each for the components GT, GB, EM1, PM, EM2 and P2 in Figure 3.11

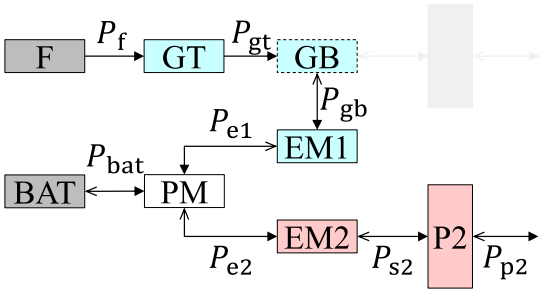

Figure 3.11: Serial hybrid layout with a gas turbine, taken from the 2018 paper by De Vries et al. [35] The boxes indicate the different components, whereas the arrows indicate the power paths. In the case of the FC propulsion system considered here, the GT is replaced with the FC and the GB and EM1 are removed.

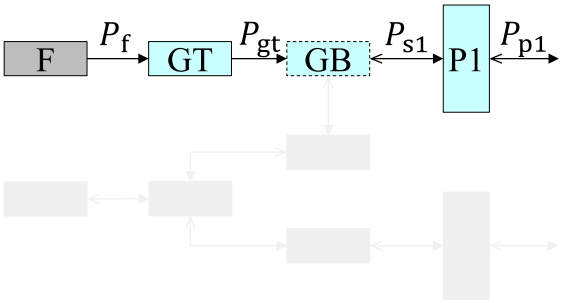

Figure 3.12: Conventional gas turbine propulsion system layout, as defined in the hybrid branch of the Initiator. [35]

The hybrid sizing process in the Initiator consists of two main parts: 1. a wing/power loading determination and 2. a mission analysis. The methodology of the first part is in principle equal to the standard way that this is done in aircraft design, i.e. there are a number of constraints (such as cruise or one-engine-inoperative (OEI) conditions) which together form a feasible design space, from which a design point is selected. The difference here is that this is done for each component (as well some power paths) separately, in order to size all parts of the system in terms of their power.

The goal of the next step is to determine the energy required from both power sources, as well as checking whether all components are indeed able to deliver enough power to complete the mission. Note that for the battery, there are two potential sizing conditions: either according to the power or the total energy that it must deliver. The Initiator checks which one results in a larger mass and takes that as the sizing condition. Further details regarding the power control parameters that the user must provide are given together with the sizing study in section 4.1.

3.4.2. Changes Made to the Hybrid Initiator Code for the Implementation of the FC System Model

Ideally, the FC system should be implemented as a new engine type, alongside the gas turbine. However, as this would require large changes, it was instead decided for this thesis project to ”hijack” the gas turbine engine type by adding additional if-statements for FC aircraft. In terms of the definition of parts in the Initiator, a hybrid system consists of two different engine types: the turbogenerator, containing the components GT, GB and EM1 and the electroprop, containing the EM2 and P2. This allows more complicated layouts, for instance with only two turbogenerators under the wings and a distributed propulsion system consisting of electroprops on top of the wings. However, in this thesis the entire system is placed in the same location under the wings, in the form of the FC engine described in the

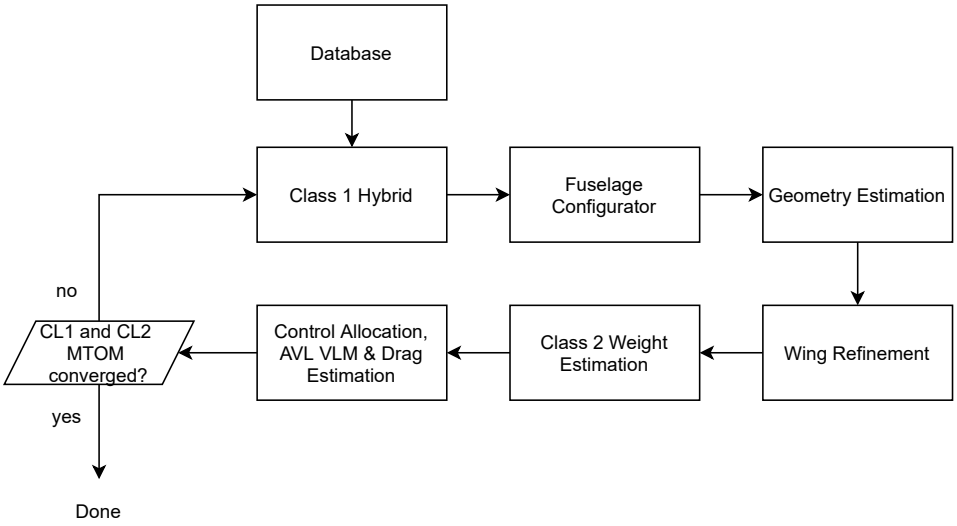

Figure 3.13: Convergence loop of the hybrid branch of the Initiator. Note that the Class 2.5 methods are turned off, due to which there are no top-level nested loops. Except for the last one, every box corresponds to a separate module.

previous chapter. Therefore, in the aircraft input file, the same amount of turbogenerator and electroprop parts is placed at the same locations in pairs under the wings.

Figure 3.13 shows the convergence loop of the hybrid sizing process. Note that no nested loops are present, as the Class 2.5 methods are turned off. This is because the additional accuracy often comes at the cost of convergence problems, with these methods being very sensitive to input parameters. Each block corresponds to a separate module in the Initiator code, except for the last block, where several have been bunched together as they are not specifically relevant for a FC system. Below, the most relevant modules are shortly described, and the most important changes made are explained.

Database

The Database module is run once, at the beginning of the process. Its task is to load a number of reference aircraft and engine databases, as well as a number of constants and control parameters that are relevant to the hybrid sizing process. The most important change here is that the efficiencies of the generator and gearbox, which are loaded as constants, are set to 1, effectively turning these components off. Furthermore, an initial FC efficiency is set equal to 60% for the first iteration of the process.

Class 1 Hybrid

The first module of the loop is the Class 1 Hybrid module. Normally, a Class 1 estimation just consists of the determination of a design point in terms of wing- and power loading values, as well as of the main weight figures. The empty mass (OEM) is based on statistics, and fuel fractions are then used together with the payload to arrive at the maximum takeoff mass (MTOM). However, in the hybrid case, this is more complex, as the system consists of many interacting components. As described in the previous subsection, a mission analysis needs to be run in order to determine the fuel and battery masses. Whereas for the first run, the OEMexBat (empty mass excluding the battery) is determined from statistics using conventional aircraft, it is subsequently taken from the Class 2 results of the previous iteration. The first step in the hybrid Class 1 method is the determination of a power loading for each of the components. This is followed by a mission analysis, which directly results in a fuel mass. As explained before, for the battery mass, both the mass required for the energy, as well as the mass for the design power loading (and therefore power) need to be taken into account, with the higher one being the required one.

For the gas turbine (and therefore the FC, in this case) two power loading graphs are produced: a direct and a corrected one, with the latter being decisive for the sizing of the component. It consists of two corrections. Firstly, the throttle parameter ξ, which is the second power control parameter that the user must provide (next to Φ), needs to be taken into account. If this is lower than 1 for a certain constraint, it means that the component needs to provide this power at some percentage of its maximum power, i.e. that there is a power reserve. This reduces the corrected power loading. Secondly, the effect of the altitude on the gas turbine power needs to be accounted for through a power lapse. This is where one of the major assumptions for the FC system as considered in this thesis comes into play. The power lapse is disabled, meaning that a FC produces the same power at every altitude. This is only valid because, as explained in chapter 4, it is ensured that the sizing condition for the FC is always cruise, where it runs at or slightly below its maximum power. In terms of the atmospheric conditions, this is also the most severe phase, as the air pressure is the lowest. Since the compressor is sized for this, it means that at any lower altitude the system will still be able to provide the same power.

Fuselage Configurator
In this module, the fuselage is built around the passenger cabin and, if required, the hydrogen tank. As mentioned previously, the tank sizing method that was in development during this project could not yet be used fully in combination with the FC system. Here, only the part of the code that places the tank behind the cabin and stretches the fuselage accordingly was used. For the tank sizing, an alternative, simple method was implemented, which assumes a cylinder with spherical end caps as the shape. The starting point is the fuel volume, which follows from the known fuel mass and its density. Assuming a certain volumetric storage density, this leads to a tank volume. Next, it is assumed that the tank radius is equal to 95% of the fuselage radius. If the fuel volume is larger than the volume of a sphere with this radius, then a cylindrical part is added in the middle. In any case, a tank length is obtained, leading to the required extension of the fuselage length.

Class 2 Weight Estimation
In the Class 2 module, the mass of each part is estimated, leading to a value for the OEMexBat. A value for the MTOM is also required as an output, as the overall sizing process is based on the convergence of this parameter. It is obtained by adding the fuel and battery masses from the Class 1 estimation to this new OEM. In this module, the Python script corresponding to the FC system sizing process presented in section 3.1 is run, in place of the Class 2 estimation of the gas turbine mass. Note that this process is a lot more detailed than most of the other Class 2 methods, which consist mostly of semi-empirical statistical equations. Note also that the mass of the electric motor, being an integral part of the FC engine from Figure 2.2, is estimated automatically, as it is contained in the electroprop part of the input file. The tank and the battery, on the other hand, are not yet implemented as separate parts of the aircraft object. The tank mass is estimated under the ”fixed equipment” category, by multiplying the fuel mass with a constant value for the gravimetric storage density. A typical value of 0.6 is assumed for this parameter. [34] Its centre of gravity (CG) is taken into account. In opposition to this, the effect of the battery mass on the CG is ignored. That is because a battery is much more flexible in terms of its shape, meaning that it can be spread over various parts of the aircraft more easily, for instance inside the wing or below the cabin floor. Even though the safety concerns related to this should be investigated, it can be said that it will be possible to integrate the battery into the airframe in a way that would not negatively affect the stability.

3.5. Validation of Sizing Methods

An important aspect during the development of any modelling approach is the validation of the applied methods. In this thesis, only very limited validation activities could be conducted due to the lack of relevant aircraft in the real world. The first such activity is with regards to the specific power of the FC system, which is one of its main parameters. It expresses in kW/kg how much power the system can produce per kg of mass. This value is often used in literature to estimate the mass of the system, given a certain required power. It is often based either on experience or a rough literature review and is usually in the order of magnitude of 1 kW/kg. Figure 3.14 shows this parameter as a function of the cruise altitude and the Mach number. At lower speeds and higher altitudes, the compressor becomes heavier as by default, it always needs to provide sea-level pressure to the stack. Over a reasonable range of values, the resulting specific power is indeed of the expected order, which in turn means that

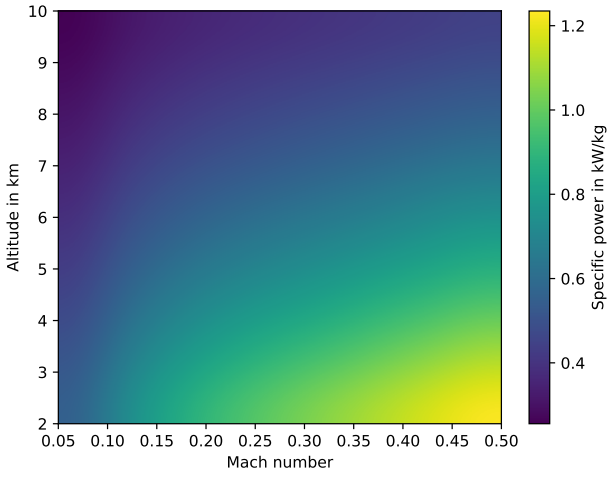

Figure 3.14: Specific power resulting from the propulsion system model alone, plotted at different altitude and Mach numbers. Both parameters have a direct influence on the compressor inlet pressure. With the default setting for the compressor pressure ratio, this has a direct influence on the system mass and therefore the specific power.

the resulting FC system mass can be considered realistic. Therefore, the fully physics-based approach developed in this thesis, which includes the sizing of all subsystems, is, at the first level, sufficiently accurate.

Next, the distribution of the total mass along the subsystems of the FC system and their components can be considered. Such data is difficult to find in open literature. For the PEM stack, two suitable data sets could be found, which are shown in Figure 3.15. While the exact numbers don't match, it is immediately clear that the bipolar plates are the biggest contributor, followed by the endplates. This makes intuitive sense, as both are metal plates with a certain thickness. But also in general, bipolar plates are often said to be the heaviest part. While the thin MEA doesn't contribute much, the mass of the bolts varies considerably, between around 1 and 17%. This is to be expected, as the design of the bolts is not directly connected to the performance of the stack. Note that this distribution is not affected by input parameters such as the output power due to the constants used in the mass model. Regarding the BOP components, the only mass distribution that could be found in literature is shown in Figure 3.16. It is presented in a paper by Bradley et al. [36] and relates to an experimental UAV. Although this severely limits the applicability to the type of aircraft considered in this thesis, a general trend can again be seen. The heaviest component is the compressor, followed by the heat exchanger. This former is also confirmed in a general way by other researchers, who do not show concrete numbers.

Out of the components of the FC system, the electrically-driven centrifugal compressor is also the only one for which mass data of commercially available examples can be found. A comparison between the data and the model implemented in this thesis is shown in Figure 3.17. Note that the range of compressor powers is orders of magnitude lower than what is required for a transport aircraft. Nonetheless, a good agreement to the data can be seen. One of the main constants that affect the slope is the electric motor power density. In this case, it is set to 2.2 kW/kg, which is within the range of currently available technologies.

Since the Initiator has been under continuous development at the faculty for many years, all other aircraft sizing aspects can be assumed to already be validated sufficiently. Nonetheless, for the sizing example presented in detail in the next chapter, the conventional reference aircraft was also re-sized using the conventional branch of the program, in order to verify its accuracy.

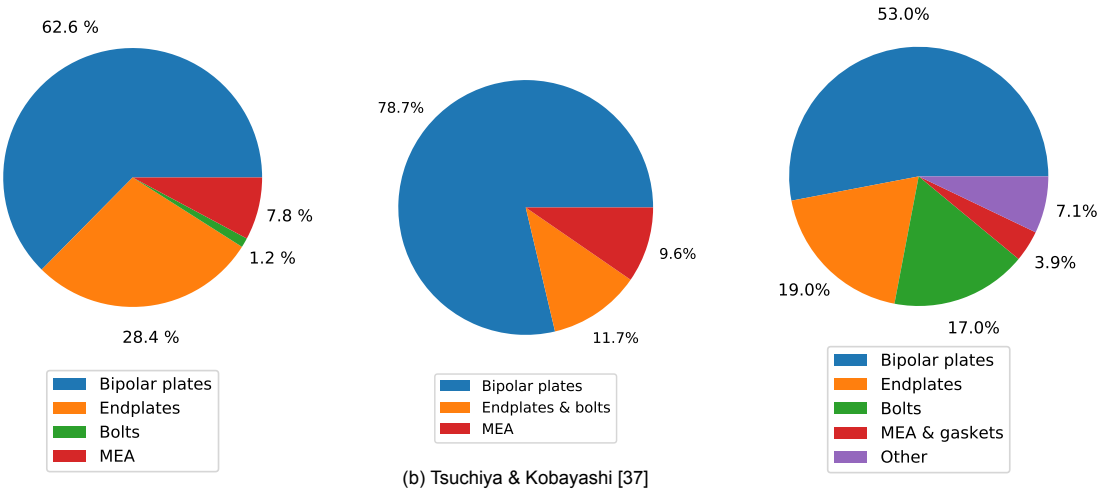

(a) Own model (b) Tsuchiya & Kobayashi [37] (c) Jayakumar et al. [38]

Figure 3.15: Comparison of the breakdown of the stack mass of the model developed here with two examples from open literature. Note that the input parameters such as the total power are irrelevant, as they do not affect this distribution due to the constants used in the mass model.

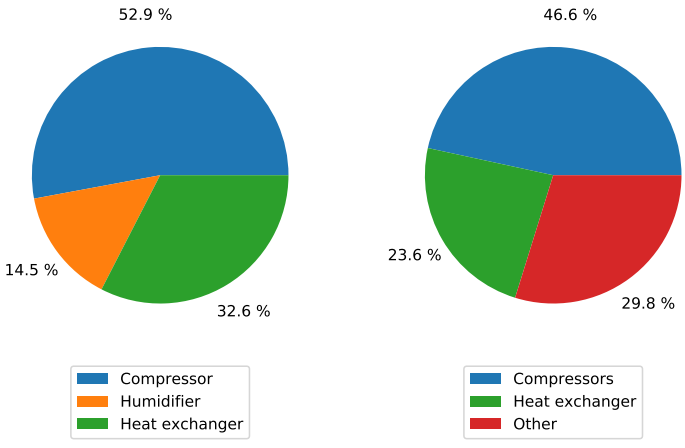

(a) Own model (b) Bradley et al. [36]

Figure 3.16: Comparison of the breakdown of the BOP masses from the model developed here with the only equivalent example that could be found in open literature. Note that the latter is with regard to a UAV, whereas this thesis focusses on CS25 aircraft. Nonetheless, the general trends can be compared.

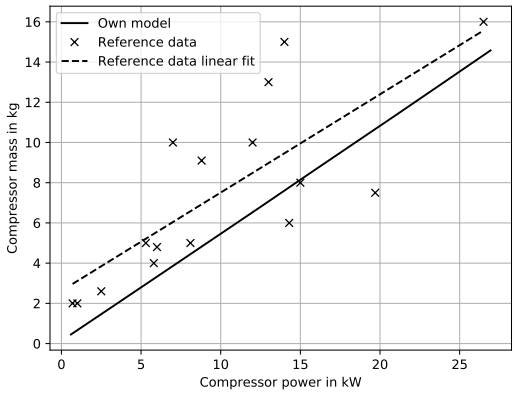

Figure 3.17: Comparison of the compressor mass resulting from the model presented here with openly available data from commercial electrically-driven FC compressors. Note that the x-values are at a different order of magnitude than what would be required for a transport aircraft. Nonetheless, the general trend can be used for the purpose of validating the model.

4

Results

In this chapter, the results obtained with the FC system model and its subsequent integration into the Initiator are described and analysed. In the first section, an existing passenger aircraft is used as a sizing example. Its characteristics and resulting design parameters are compared with those generated using the Initiator, both for a conventional and a FC-powered version. This is followed by sensitivity studies in section 4.2 and section 4.3. While the former focusses only on the system level, the latter presents such studies on the level of the complete aircraft.

4.1. Example of an Aircraft Sizing Study: Fuel Cell-powered ATR 72-600

This section contains the results of the sizing study performed using the Initiator and the FC system model. The ATR 72-600, a regional turboprop aircraft, was used as the reference. Due to the large number of inputs and the complexity of the Initiator, achieving convergence of the sizing process was an extensive task. Although it would have been valuable to consider other aircraft, such as for example single-aisle medium-range turbofan aircraft, the time constraints of the thesis did not allow for this.

Two sets of results are considered here. The first set concerns an ATR 72 sized using the hybrid branch of the Initiator. One should expect close resemblance with the reference aircraft, but not necessarily an exact match in every characteristic. That is because in general, the only inputs are mission and basic design parameters (such as the spanwise location of the engine), instead of specific constraints or predefinitions of certain parts of the aircraft. For instance, the planform of the wing is not given as an input, meaning that it will be defined using the methods contained in the Initiator, which will most likely not exactly reproduce the original one. In other words, the goal is not to exactly reproduce the ATR 72, but to size an aircraft that has the same performance and payload characteristics. The purpose of this set is to check the validation of this branch of the Initiator w.r.t. to parts that are not specific to a FC or any other hybrid configuration. Although this was already done during the development of the Initiator, it is good to verify this specifically for the example used in this thesis. Note that for this purpose, a conventional aircraft, in this case one with two turboprop engines, can indeed be sized using the hybrid branch, as mentioned before. In that case, the propulsion system layout only contains the components GT, GB and a primary propeller P1, as shown in Figure 3.12.

The second set concerns an ATR 72 with two FC engines placed at the same absolute locations as the original turboprops and a liquid hydrogen tank placed aft of the cabin, hereafter to be called FC-ATR 72. This means that the hybrid branch of the Initiator was used together with the FC system model and, otherwise, exactly the same inputs. Therefore, this aircraft is able to fly the same mission as the real ATR 72. The purpose of this is to demonstrate the capabilities of the propulsion system model in the context of a complete aircraft sizing scenario. Also, this allows some more general statements about FC aircraft to be made, in order to address the third research question, which was shown in section 2.3. Furthermore, it provides a base for sensitivity studies on the level of the complete aircraft, which are

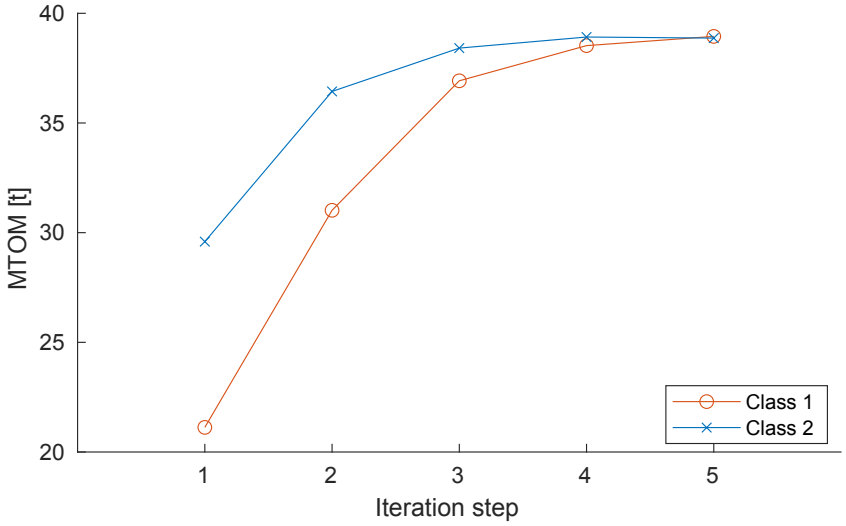

Figure 4.1: Convergence history of the FC-ATR 72, in terms of its MTOM. In the last iteration, the difference between the MTOM values from the Class 1 and Class 2 methods dipped below $5 \cdot 10^{-3}$, which is the user-specified tolerance. The duration of this complete process was around 143 seconds.

presented below in section 4.3.

In subsection 4.1.1, all results are described and compared in general, for both sets. This is followed by an explanation of how the power control inputs ξ and Φ were selected, as well as of the resulting power loadings and mission power profiles in subsection 4.1.2. Although the latter is not in its entirety specific to the FC propulsion system, it is included here in detail due to the amount of work that it required.

4.1.1. Description of the Overall Results of the Aircraft Sizing Study

The main numerical results of the sizing studies are shown in Table 4.2. The first column shows the values of the original real aircraft, whereas the two following columns show the two sets of results as described in the introduction of this section, respectively. Convergence was achieved in five iterations for the FC-ATR72, as shown in Figure 4.1, and in three for the conventional aircraft (as shown in Figure A.1). Using a high-end consumer laptop, the former took around 143 seconds, and the latter only around 47 seconds. This illustrates the high level of detail of the modelling approach for the FC propulsion system.

Before comparing the values contained in this main table, a few remarks should be made. For the first column, the values are in general taken from brochures[1] that can be found on the website of ATR, the manufacturer of the original aircraft. The engine mass is obtained from the PW127M variant in the EASA type-certificate data sheet. The maximum power is equal to twice the highest value found in the brochures, which is the one-engine-out (OEI) take-off power, times an assumed propeller efficiency of 80%. Therefore, this is not a continuous, but a peak power figure. Even though using this OEI-specific power setting on both engines might not be a part of normal operations, it does give an indication of the theoretical capabilities of the aircraft. Note that a value for the gas turbine efficiency could not be found.

For both the second and the third column, there is only a single input mission. Its main parameters are presented in Table 4.1. This mission is at a slightly higher range than the harmonic range of the reference aircraft, which means that the payload is slightly reduced, with 72 passengers being the maximum design capacity. This mission had previously been used as the main one in the existing input files of the Initiator, meaning that it was convenient to keep using it here, for instance to compare with previously obtained results. Note, that the Initiator does have the ability to handle multiple input missions, as would be the case for a real aircraft sizing scenario. In that case, it would determine the

[1] mainly from `https://www.atr-aircraft.com/wp-content/uploads/2020/07/Factsheets_-_ATR_72-600.pdf`

Table 4.1: Mission parameters used for both ATR 72 sizing studies. These are equal to one of the points of the payload-range diagram of the reference aircraft.

Parameter	Value	Parameter	Value
Passengers	70	Take-off distance	1333 m
Payload	6650 kg	Approach speed	58.1 m/s
Cruise Mach number	0.408	One-engine-out (OEI) ceiling	4.33 km
Cruise altitude	7 km	Loiter time	45 min
Design range	1530 km	Diversion range	185 km

harmonic mission and use this as the base for all computations. However, to simplify the modelling, this capability was not used in this thesis. For the third column of Table 4.2, it is important to note that the OEM includes the battery and that the engine mass is equal to the FC engines plus the nacelles.

When comparing the first two columns, one can see that the OEM is almost identical, which means that the mass estimation of all components that are not related to a hybrid system is rather accurate. A bigger difference can be seen in the MTOM, which is mainly caused by the significantly higher fuel mass of the reference aircraft. Another parameter that differs significantly is the maximum propulsive power, leading to a lower power loading as well as heavier engines. Unfortunately, the specific reason for these inconsistencies could not be found. One possibility is that this is caused by the simplified engine model which is used in the hybrid branch, instead of the other more detailed model available in the Initiator. Despite this, meaningful statements about these figures can still be made when comparing the second and third column. Furthermore, the fuselage length and the wing loading of the first two columns are close. The latter is tuned mainly with the input CL_{Max} values.

Looking at the results of the FC-ATR 72, one will immediately notice a considerable increase in the MTOM. This is due to the OEM which has more than doubled. While some structural elements have certainly become heavier as a consequence of the snowball effect, the main contributors to this drastic change in empty mass are the engines and the battery. The FC engines are more than eight times as heavy as the original turboprops, which is not only due to the higher cruise power, but also due to the comparably much lower power density. Furthermore, the maximum propulsive power has increased as well, while having roughly kept the same power-loading as in the conventional sizing study.

Despite this higher take-off mass, the fuel mass is still lower than that of the kerosene in the reference aircraft, which can be expected due to the higher gravimetric energy density of hydrogen. Even though a doubling in empty mass seems dramatic at first, one should keep in mind that this aircraft has exactly the same mission and performance capabilities as the reference aircraft and that the design has converged. Furthermore, as explained more in detail in section 4.3, varying the range will only have a small effect on the empty mass, meaning that there is also some flexibility in the design point. More attention will only have to be paid to those inputs which increase the maximum power, as that would significantly change the engine mass and hence the OEM. Therefore, the larger total mass is not necessarily a problem when considering the bigger picture, at least from the point of view of the technical feasibility. Also shown in the table is an increase in fuselage length by roughly 5.4 m, which is the length of the liquid hydrogen tank. Furthermore, it is interesting to note that the difference in the efficiency of the main power converter (i.e. the gas turbine or fuel cell) is less than expected. The low FC system efficiency is mainly due to the large power utilisation of the compressor. In fact, the cell efficiency during cruise is equal to 49%.

Table 4.3 shows a breakdown of the component masses that are related to the propulsion system of the FC-ATR 72, for both engines combined (where applicable). It is interesting to note that the FC systems weigh roughly as much as the electric motors. Furthermore, the hydrogen tank is actually heavier than the fuel itself. Figure 4.2 and Figure 4.3 show an isometric and a top view of the FC-ATR

Table 4.2: Main results of the FC-ATR 72 example sizing study, compared with the existing reference aircraft and a corresponding conventional one sized with the hybrid branch of the Initiator. The percentage values are w.r.t. to the previous column, respectively.

	Original	Conventional in Initiator	Fuel cell in Initiator
MTOM [kg]	23000	21908 (-4.7%)	38870 (+77.4%)
OEM [kg]	13450	13477 (-0.2%)	31265 (+132.0%)
FM [kg]	2900	1781 (-38.6%)	956 (-46.3%)
BM [kg]	-	-	2882
Engine mass (all) [kg]	964	1346 (+39.6%)	8146 (+505.2%)
Fuselage length [m]	27.2	26.1 (-4.0%)	31.5 (+20.7%)
Max propulsive power [MW]	3.24	4.83 (+49.1%)	8.51 (+76.2%)
Max propulsive power loading [N/W]	0.0696	0.0414 (-40.5%)	0.0448 (+8.2%)
Wing loading [N/m^2]	3699	3690 (-0.2%)	3648 (-1.1%)
GT/FC efficiency (η_{GT}) during cruise	?	0.38	0.43 (+13.2%)

Table 4.3: Mass breakdown of the propulsion system components (in the wider sense) of the FC-ATR 72. The summation of the left half corresponds to the engine mass shown in the Table 4.2.

Component	Mass in kg	Component	Mass in kg
FC stacks	1834	Battery	2882
Compressors	876	Hydrogen tank	1594
Humidifiers	447	Cables	233
Heat exchangers	792		
Electric motors	3618		
Nacelles	518		

72, respectively. The latter also shows a comparison with the conventional aircraft sized in the Initiator. What can be seen immediately is the space behind the passenger cabin, where the hydrogen tank is placed. Moreover, the effect of the identical wing loading and aspect ratio at an increased MTOM can be seen in the increase in the chord lengths and the span. Finally, despite having a larger moment arm, the horizontal tail surface is larger. This not only due to the increased mass, but also the location of the hydrogen tank far away from the wing. Note that neither the tank nor engines are rendered in the isometric view. This is because the 3D rendering capabilities of the Initiator were not used in the FC system and tank models.

4.1.2. Description of the Power Control Input Parameters Used for the Sizing Example

Whether or not the design of the FC-ATR 72 converges is highly dependent on the power control parameters ξ and Φ. The values used to generate the results shown in the previous subsection are presented in Table 4.4. In the first half of the table, the parameters used for the determination of the component-wise power loading are shown. A selection of the most relevant power loading diagrams resulting from these is shown in Figure 4.4. The values of ξ and Φ are chosen for each constraint according to three general principles:

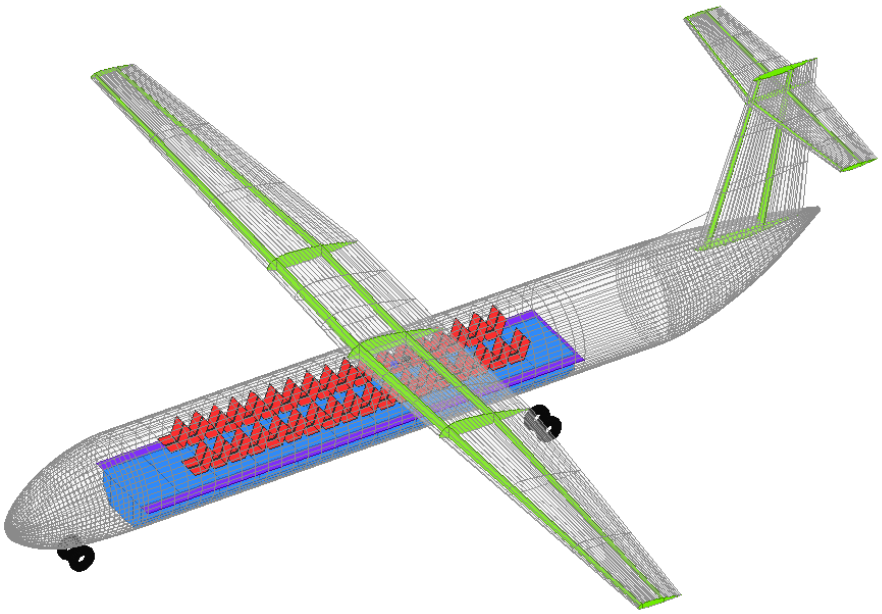

Figure 4.2: Isometric view of the FC-ATR 72. Neither the hydrogen tank nor the engines are shown here, for reasons explained subsection 4.1.1.

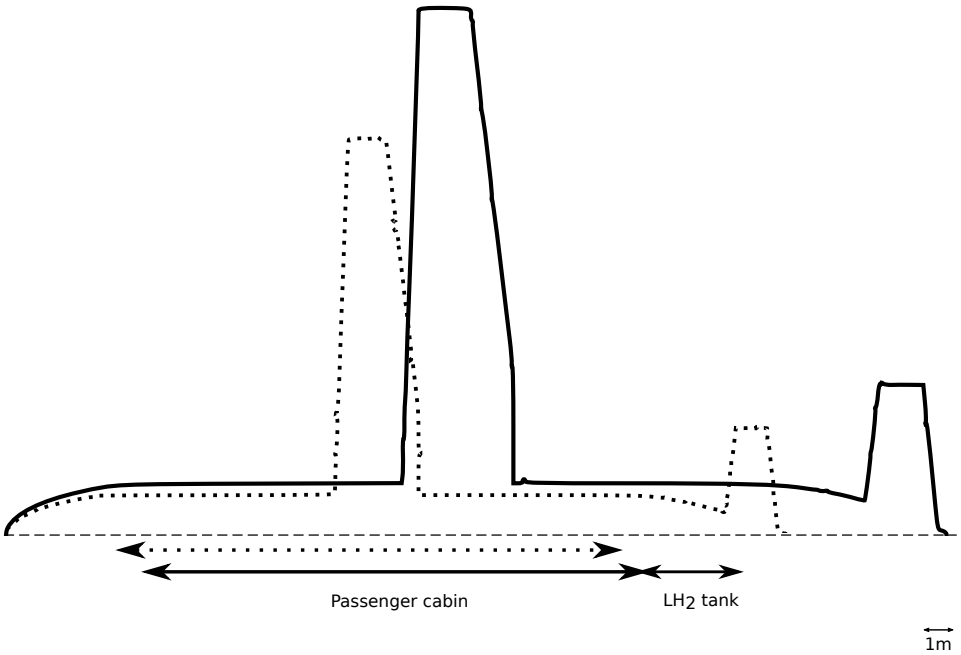

Figure 4.3: Top of view of the FC-ATR 72. Note that the engines are not shown. This is because it was generated manually from a top view of the 3D model of Figure 4.2. The dotted lines indicate the conventional ATR 72, sized using the hybrid branch of the Initiator.

1. The FC should always work as close as possible to its maximum power (i.e. ξ should be as close as possible to 1), except for the landing

2. The battery should only be active during the phases that require more power than cruise, with a Φ which is as low as possible

3. For the FC, the cruise constraint should be sizing

The first two principles encompass the general idea of the hybrid configuration for a FC aircraft. The FC should be able to provide enough power for cruise, but not significantly more, in order to limit the mass of the propulsion system in connection with the low power density of FCs. During the other flight phases, it will run at the same power. Φ in turn should be as low as possible to limit the mass of the batteries.

The third principle is not necessarily required for a hybrid system, but is used in this thesis project to simplify the situation. If another constraint was sizing for the FC, then the system would have to be sized twice, i.e. by two different constraints, with different atmospheric conditions. On one hand, the sizing constraint would result in the maximum power that the FC system would have to produce, i.e. it would determine the total stack area and therefore also the mass of this component. On the other hand, the cruise constraint would in that case be sizing for the BOP, as at the cruise altitude, the most severe atmospheric conditions (mainly w.r.t. the pressure) are encountered. Consider an example where a constraint at sea-level was sizing: in that case, no compressor would be required at all. The compressor would however still be required for cruise. To satisfy this condition, one might have to reduce ξ at cruise in order to force the constraint to become sizing. This was indeed the case for this sizing study, as shown in the next paragraph.

In Figure 4.4a (the corrected power loading diagram for the FC), the cruise constraint is sizing, with the OEI balked landing constraint being just slightly higher. To achieve this, ξ during cruise had to be reduced to 0.9 and Φ during this OEI constraint had to be increased to 0.42, as shown in Table 4.4. The effect of the former can be seen when comparing with the non-corrected power loading diagram of Figure 4.4b. As described in subsection 3.4.2, the only correction applied between Figure 4.4a and Figure 4.4b is due to ξ. Although this value for ξ is somewhat in contradiction with the first principle from above (as it is smaller than 1), it is necessary to satisfy the third principle. Nonetheless, some other positive effects can be derived from this value of ξ. Firstly, in this way the fuel cell has a certain reserve in terms of power during cruise, meaning that it could for example still climb in an emergency situation where there is a problem with the battery. Secondly, this also reduces the battery mass, as this reserve can be used during the high-power phases such as climb. Thirdly, the FC efficiency during cruise is increased, reducing the fuel mass. Note that in the power loading diagrams in this subsection, only the design point for maximum wing loading is shown, to minimise the wing size. Although the Initiator is capable to also consider other design points, for instance to minimise each of the propulsion system components, this is not used here, again in order to simplify the situation.

An important thing to realise at this point is that for the FC-ATR 72, the battery is in fact sized according to its power and not its energy requirement. Even though it is a close call (2401 kg for energy and 2882 kg for power), it means that Figure 4.4d, the power loading diagram of the battery, must be considered as well. As can be seen, the battery is sized by the take-off constraint. Lowering the corresponding Φ would reduce the battery mass. However, this would also lower the corresponding line in the corrected FC power loading graph, as the FC would then have to take over more power for that constraint. This in turn would violate the principle that the FC should be sized by cruise, as the OEI balked landing and the TO constraint intersect the given wing loading practically at the same position. This means that the take-off constraint is, in this situation, already optimal. Considering all diagrams of Figure 4.4 together, one can see that the other constraints are not currently active, which is why their Φ was arbitrarily set at 0.4. Finally, note that the electric motors are sized by the OEI balked landing constraint as well, as shown in Figure 4.4c.

Table 4.4: Hybrid system power control input parameters used for the FC-ATR 72 sizing study.

Power loading constraint	ξ	ϕ	Mission analysis phase	ξ_{start}	ξ_{end}	ϕ_{start}	ϕ_{end}
Cruise	0.9	0	Climb	0.8	1	0	0.3
Landing	0	0	Cruise	-	-	0	0
Take off	1	0.4	Descent	0	0	0	0
Balked landing	1	0.42	Diversion climb	0.9	1	0	0.1
OEI ceiling	1	0.4	Diversion cruise	-	-	0	0
OEI 2nd segment	1	0.4	Diversion descent	0	0	0	0
OEI initial	1	0.4	Loiter	-	-	0	0
OEI trans	1	0.4					
ROC AEO	1	0.4					

Next, the choice of the parameters of the second half of Table 4.4, i.e. for the mission analysis of the hybrid Class 1 method needs to be explained. Note that for each flight phase, both parameters can be given different values for the start and the end of the phase. The basic principles are the same as for the power loading parameters: ξ should be equal to 1 or slightly lower for all phases except the descents, with Φ being bigger than zero for all climb phases. However, for the horizontal phases, ξ is solved for by the powertrain sizing methods and therefore doesn't need to be specified by the user.

The correct behaviour of the propulsion system during the mission can be verified by considering Figure 4.5. Figure 4.5a contains the time history of the power control parameters. Indeed, ξ and Φ are exactly as specified for the climbing phases. For the main cruise phase, ξ is roughly equal to 0.95, reducing very slightly as some of the hydrogen is consumed. This is in line with the ξ at cruise defined in the power loading part. During the loiter phase, ξ is significantly lower, as the horizontal flight there is done at a lower altitude and speed. These statements are also consistent with Figure 4.5b, where the power sources along the flight are shown. Note that the different lines in both subfigures correspond to the five iterations required to achieve convergence, as shown in Figure 4.1. With each iteration, the MTOM increased, which means that the highest line in each subfigure corresponds to the final design. It is interesting to consider the lowest fuel power source line in Figure 4.5b (i.e. the one that corresponds to the first iteration). Its distance from the next line is much larger than for later iterations, which is not the case for any of the lines in the first subfigure. In fact, this is due to the initial, overly optimistic guess for the efficiency of the FC system of 60%, mentioned first in subsection 3.4.2. In combination with the initial low value for the MTOM, which is mostly a result of the statistical OEM estimation derived from conventional aircraft, this causes a much lower fuel consumption in the first iteration. Subsequently, the FC efficiency and MTOM change to more realistic values, resulting from the FC system model and the Class 2 weight estimation respectively. This then causes an instantaneous jump in the fuel power.

The values shown in Table 4.4 were determined either by adhering to specific design choices (such as requiring the FC to be sized by the cruise constraints) or through a rough manual optimisation, with the minimisation of the battery mass as its goal. Better results, in terms of a smaller propulsion system and a lower fuel mass, could certainly be achieved through a numerical optimisation of this problem and by considering other options for some of the choices. However, automating this optimisation presents a very complex problem from a mathematical point of view and is therefore far beyond the scope of this thesis project.

Note that in the choice of the power control parameters, it can happen that the power loading becomes incompatible with the mission analysis if the values from both sides of Table 4.4 are too different. For instance, it could happen that the power of the battery, resulting from its power loading, becomes too small to satisfy the Φ values during the climb phase. In that case, the Initiator will automatically scale up this component during the mission analysis, to ensure that it always converges to a consistent,

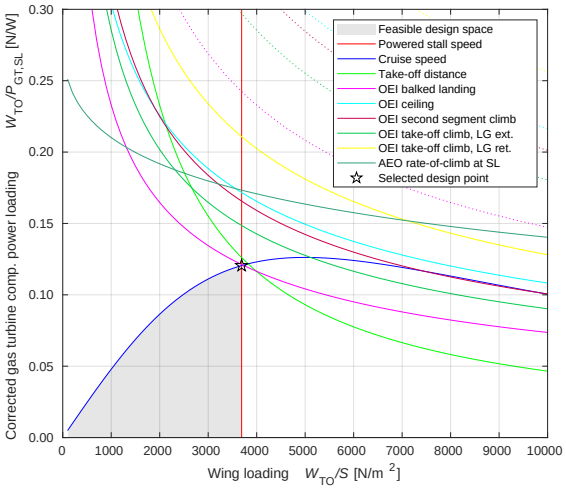

(a) Corrected FC component power loading

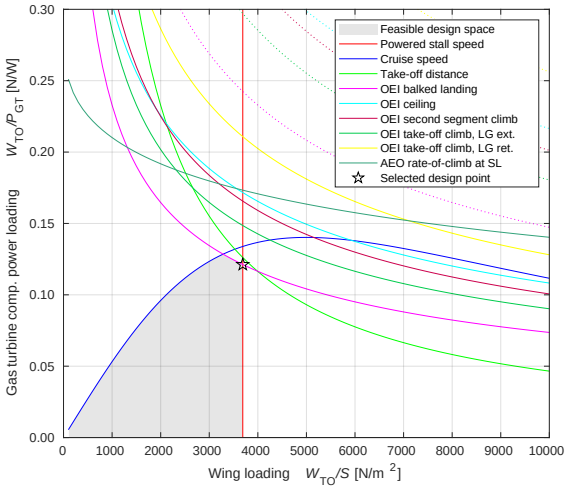

(b) FC component power loading

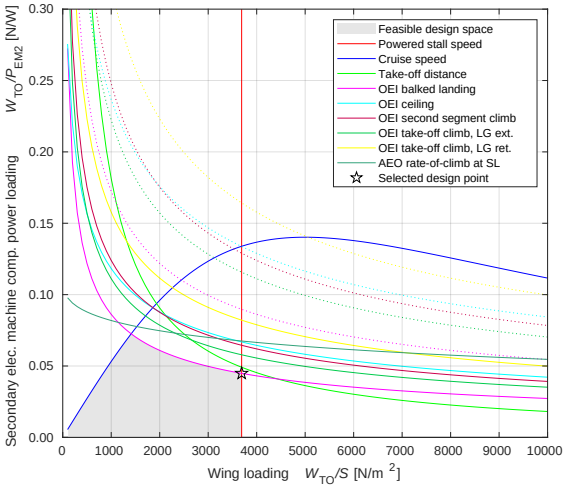

(c) Electric motor power loading

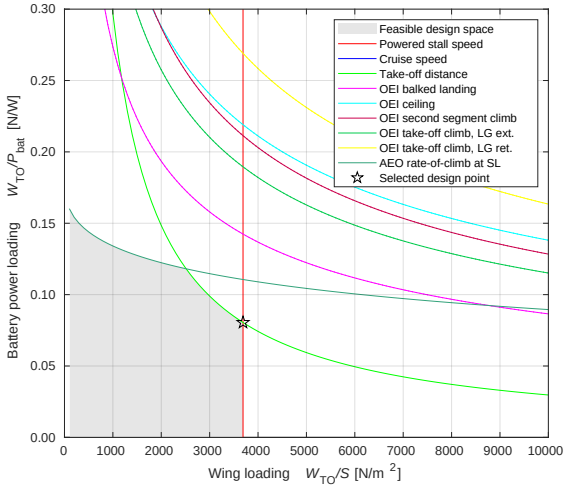

(d) Battery power loading

Figure 4.4: Power loading diagrams for various parts of the FC-ATR 72 propulsion system, resulting from the power control parameters shown in Table 4.4. All power loadings are related to the components and not the power paths. The design point corresponding to the maximum wing loading is shown as well. Note that the y-axes of Figure 4.4a and Figure 4.4b mention a ”gas turbine”, even though they are in fact fuel cells. This was left here on purpose, to once again illustrate the way in which the FC system model was implemented in the combustion-based hybrid branch of the Initiator.

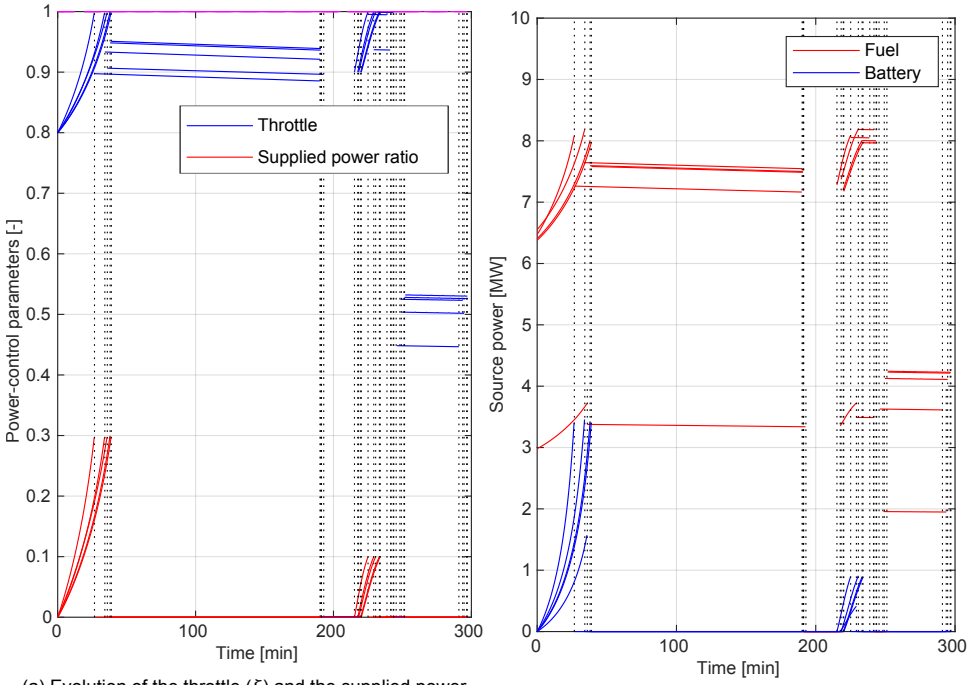

(a) Evolution of the throttle (ξ) and the supplied power ratio (Φ) along the mission

(b) Evolution of the power sources along the mission

Figure 4.5: Power profiles resulting from the Class 1 Hybrid mission analysis. The different lines correspond to the five iterations shown in Figure 4.1, which were required to achieve convergence.

feasible design. In general, it was ensured that this does not occur to a significant extent during the generation of the results presented in this chapter. Even though it will still be a valid result, the direct connection to the user inputs would be lost, making their analysis less valid.

4.2. System & Subsystem Level Sensitivity Studies

In this section, several system-level sensitivity studies are presented. These were performed by varying the inputs to the FC system model, in isolation of the complete aircraft sizing procedure. Unless mentioned otherwise, all studies were performed at an input power of 1 MW, an altitude of 5 km, a Mach number of 0.3, a cell voltage oversizing factor of 0.2 and a system voltage of 500 V. These values are in the range of what can be expected for a small regional aircraft.

The first two sensitivity studies to be presented here examine the effect of two important subsystem design parameters on the mass distribution of the FC system and its efficiency, namely the compressor pressure ratio β and the cell oversizing factor. Both are currently set as a constant, to be chosen by the user. Therefore, it is important to understand their effect on the resulting system, especially in the context of potential future numerical optimisations.

It should be mentioned why the parameters in this section are only examined on the level of the system and not of the entire aircraft. The main reason is that performing this type of study on the level of the aircraft is more complex, not only because the generation of each data point takes several minutes, but also because strong variations away from the design point of the aircraft that is considered (in this case the FC-ATR 72) can in some cases cause conflicts with some of the assumptions, causing the design to not converge anymore. This is especially the case w.r.t. the power control inputs. Although this does limit the scope of the results presented in this section, one can still reason logically at the level of the aircraft. For instance, in most of the studies, the resulting FC system efficiency is analysed as well, allowing conclusions to be made about the extended effect on the fuel mass. However, some parameters, such as the take-off distance, can simply not be examined using just the FC system model, requiring the use of the Initiator sizing procedure, as presented in section 4.3.

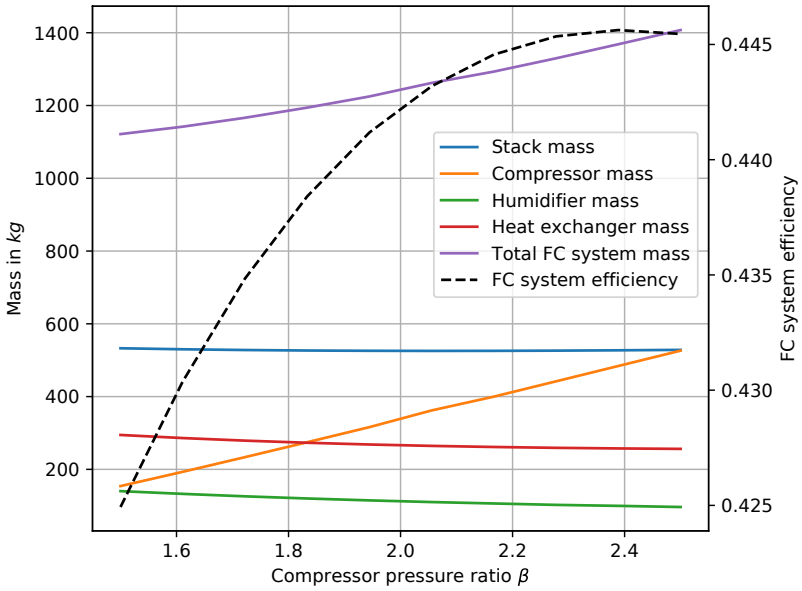

Figure 4.6: Effect of the compressor pressure ratio β on the mass distribution of the FC system and its efficiency. The range of values of the x-axis shown here is roughly equal to those that are needed to provide sea-level pressure to a stack for an aircraft flying at a typical cruise altitude and a moderate Mach number.

4.2.1. Effect of the Compressor Pressure Ratio on the FC System

In Figure 4.6, the compressor pressure ratio β is varied while the altitude is kept constant at 7 km (i.e. equal to the cruise altitude of the FC-ATR 72). At this altitude, a ratio of approximately 2.5 corresponds to the sea-level pressure. Since β is varied freely, the experimental voltage loss model has to be used. As expected, the compressor gets heavier with increasing β as it needs to "work harder". At first, one might expect the stack mass to decrease at the same time, as the voltage losses are reduced, causing an increase in cell voltage as well as power density, as shown in Figure 4.10. The latter in turn leads to a smaller cell area. Both effects together could then theoretically result in an optimal point for the total mass. Instead, the stack mass barely changes. That is because the cell area needs to in turn increase again in order to make up for an increase in the compressor power which it needs to additionally produce. At the same time, both the heat exchanger and the humidifier become slightly lighter. This is respectively due to a reduction in heat production and in the cathode inlet mass flow, both of which are due to the improved cell efficiency (see Equation 3.4 and Equation 3.6). Nonetheless, the total FC unit mass still steadily increases. Although this might suggest that β should be minimised, one needs to also take into account that the FC system efficiency is affected as well, which in turn changes the fuel mass. Therefore, this parameter should in future studies also be considered on the level of the complete aircraft.

Having made use of the experimental voltage loss model above, it is interesting to also consider a situation where no compressor is present at all. This is plotted for different altitudes in Figure 4.7. The pre-compression effect due to the non-zero Mach number is still taken into account. As expected, the stack mass increases significantly at higher altitudes as the cathode inlet pressure is reduced, causing a lower cell efficiency. This also leads to a heavier heat exchanger and humidifier. The main takeaway from this consideration is that a compressor is most likely beneficial. However, it does not necessarily need to provide sea-level pressure. A reduction of the compression ratio w.r.t. this condition would reduce the compressor mass, while causing a slight increase in the other BOP masses as well as the fuel mass. Therefore, this is another trade-off that should in future studies be performed at the level of the entire aircraft.

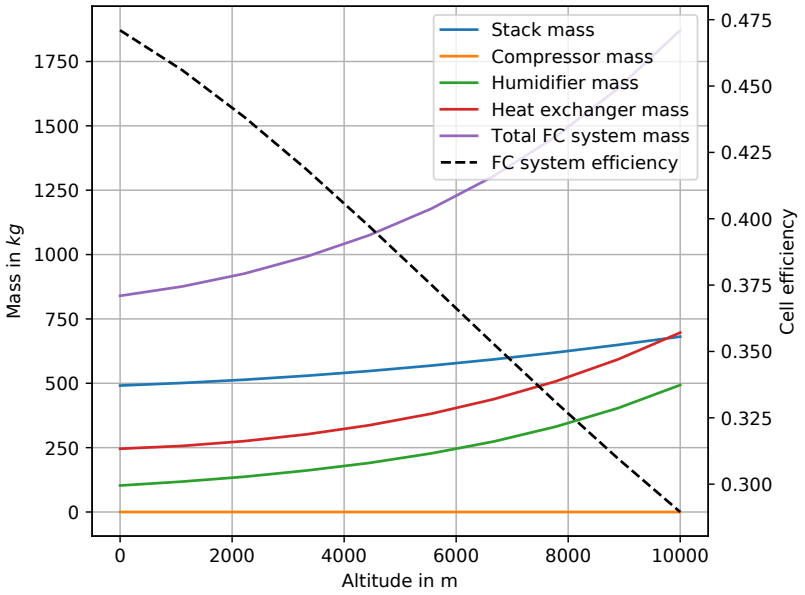

Figure 4.7: Effect of the altitude on the mass distribution of the FC system and its efficiency, given that no compressor is installed.

Considering this, one of the main simplifying assumptions in the compressor model is the fixed isentropic efficiency $\eta_{is,comp}$. The effect of a change in this parameter is shown in Figure 4.8. As expected, a more efficient compressor is also lighter, at any given altitude. Note that here, β is again chosen in the default way. Another consequence is that the power consumption of the compressor is reduced leading to a smaller stack area and therefore a lighter stack. This shows that implementing a proper loss model for the compressor would have a significant influence in terms of the overall system mass.

4.2.2. Effect of the Cell Oversizing Factor on the FC System

A similar study can be done with the cell oversizing factor as shown in Figure 4.9. This was again performed at an altitude of 7 km. The input power was also changed to 3 MW to produce a clearer result. Increasing the oversizing factor leads to a higher cell voltage but a lower power density. This is different to the effect of β, where both the voltage and the power density increase simultaneously. Instead, a bigger oversizing factor shifts the design point of the cell to the left of the polarization curve, where the efficiency is higher at the cost of a lower current density, as shown in Figure 4.10. Therefore, the stack mass increases due to a larger area, whereas the mass of the other BOP components decreases due to a reduced mass flow and heat rate. An optimal point in terms of the total FC system mass can be found around a factor of 0.25. It is interesting to compare this with the default value of 0.1 which was chosen initially. Again, the change in fuel mass must be taken into account as well in the future in order to optimise this factor considering the complete aircraft.

4.2.3. Effect of the System Voltage on the FC System

The main performance input to the FC system model, the required output power, is not interesting to consider in the type of sensitivity studies shown in this section at it simply scales up the entire system. The system voltage does however merit a short consideration, especially in connection with the number of stacks in a single FC unit. As shown in Figure 4.11, increasing this voltage in general reduces the mass of the stack since the relative effect of the non-repeating hardware is reduced. This is because if the total area is to stay constant (such that the output power doesn't change) but the number of cells reduces, the area of each cell must increase, leading to larger endplates, which then also affects the clamping bolts. Note however that the stack mass model implemented here relies on a number of constants, which means that the validity of this graph away from the centre of the x-axis becomes

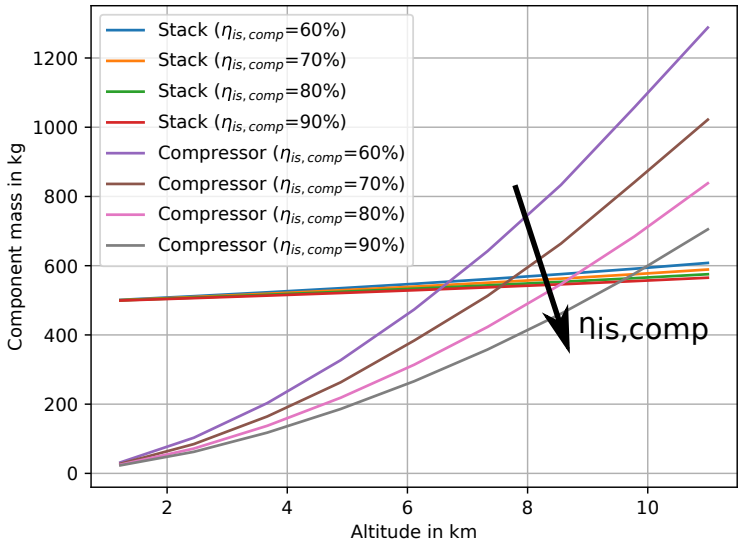

Figure 4.8: Effect of the compressor isentropic efficiency, which is currently a constant in the compressor model, on the stack and compressor masses. These are plotted for a range of altitudes as seen on the x-axis.

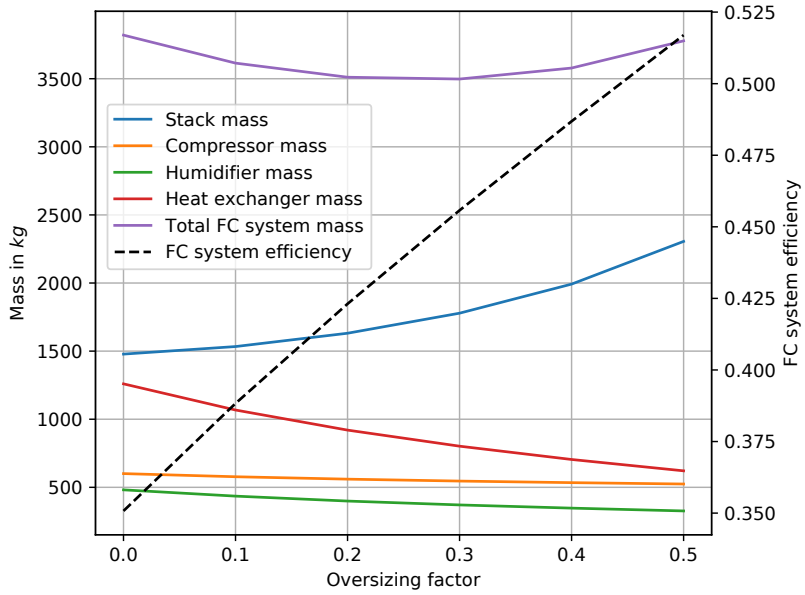

Figure 4.9: Effect of the cell voltage oversizing factor on the mass distribution of the FC system and its efficiency.

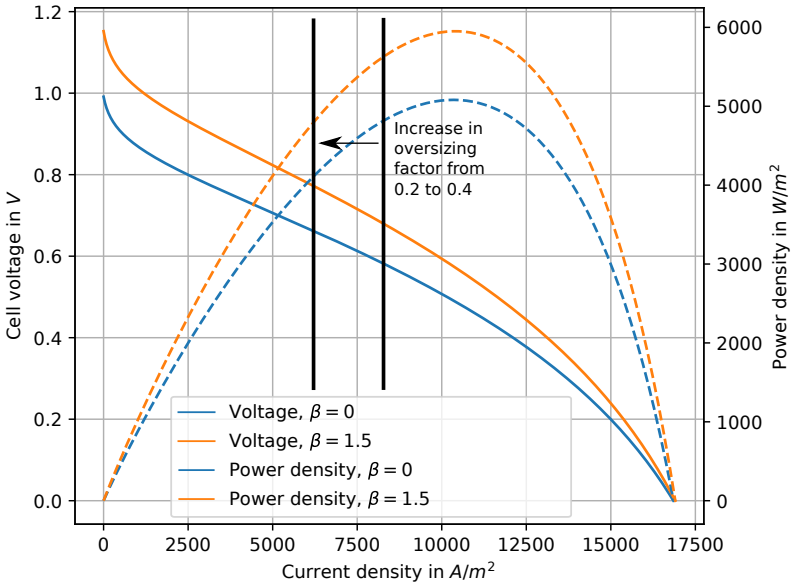

Figure 4.10: Effect of both the compressor pressure ratio β and the cell oversizing factor on the voltage and power density curves of the polarization model.

questionable, as this is the expected voltage (considering other electric transport vehicles) for which the constants were, roughly speaking, chosen. Obviously, the stack mass does not reach infinity at a low number of cells. This shows that to improve the generality of the propulsion system modelling approach, the constants of the mass models should be converted to variables. Also shown in this graph is the resulting mass for a FC unit with two stacks in series instead of just one. This essentially doubles the mass contribution of the endplates, causing a step-increase in the mass. This shows that, depending on the exact magnitude of this increase, a voltage converter might be beneficial, even though its efficiency would then have to be considered as well. This would again cause a slight increase in stack mass due to an increased power requirement.

4.3. Aircraft Level Sensitivity Studies

Thanks to the integration of the FC system model in the Initiator, sensitivity studies can also be performed on the level of the complete aircraft. This becomes especially interesting when done with mission parameters such as the range, as they cannot be examined using just the propulsion system model. All studies performed in this section were done using the FC-ATR 72. Note that one of the difficulties here is that each data point requires a full run of the Initiator, which by itself takes several minutes.

4.3.1. Effect of the Design Cruise Range and Cruise Mach Number on the Entire Aircraft

First, the effect of the design range on some of the main mass parameters is analysed. This is shown in Figure 4.12. Since only the FC runs during cruise, the fuel mass increases with the range. Note however that, to start with, this mass is already quite low, with a mass fraction of only 2.46% (see Table 4.2). Due to the snowball effect, this causes an increase in MTOM. It can also be seen that the battery mass barely changes. It only delivers power during the climbs, which means that the range doesn't affect the energy required in the battery, beyond the simple snowball effect through the MTOM. For the FC-ATR 72 though, the battery is in fact sized by the power required. This power required during climb is only very slightly increased, due to the higher overall mass.

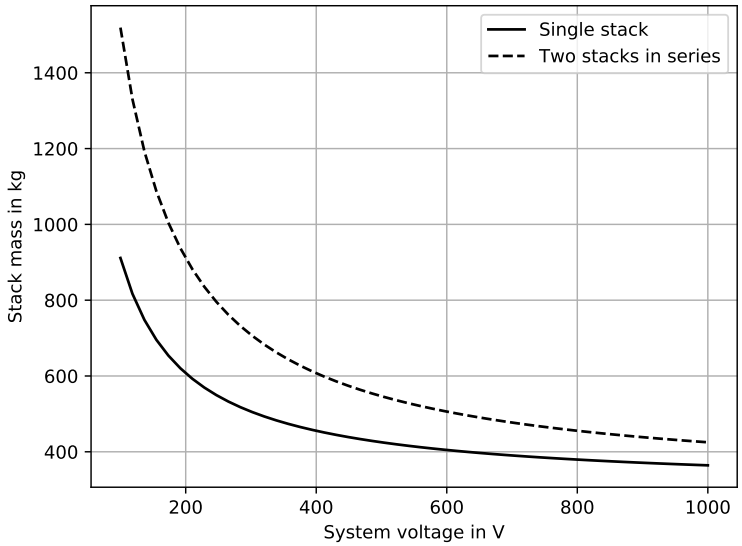

Figure 4.11: Effect of the system voltage on the stack mass, plotted for both a single stack and two stacks in series.

These results suggest that a FC aircraft is in fact less sensitive to the design range than for example a battery-electric one. At any given design point, a given increase in range will increase the energy needed for cruise. Due to the much higher gravimetric energy density of hydrogen as compared to modern batteries, this will cause only a small increase in overall mass for the FC aircraft. For a bigger change in range, the battery-powered design might become infeasible. What needs to be kept in mind for a FC aircraft though are parameters which increase the required power. As shown in Table 4.3, the FC systems and the EMs contribute roughly the same amount to the engine mass, which is already much higher than that of the original ATR. For the former, the cruise power is decisive, whereas for the latter, is it the power resulting from the OEI balked landing constraint.

Since the latter is identical for a battery-powered aircraft, the cruise power is considered next. One of the main parameters influencing this is the flight speed, i.e. the cruise Mach number. Its effect on the aircraft level is shown in Figure 4.13. As expected, the mass of the FC units increases, as more power is required during cruise to fly at higher velocities. This also directly causes more fuel to be consumed. The effect of both on the MTOM can be clearly seen. Note that only a small range of Mach numbers is shown, as the design quickly converges unless other inputs such as the power control parameters are varied at the same time. Anyway, it is difficult to compare the effect of a change in the range to a change in the Mach number, considering the bigger picture. The purpose of this figure is just to prove the effect that a change in a requirement affecting the cruise power has on a FC aircraft.

4.3.2. Effect of the Take-Off Distance on the Entire Aircraft

The next mission parameter that is of interest is the take-off (TO) distance, of which the effect is shown in Figure 4.14. Around the original distance of 1333 m, an increase in the distance causes a clear reduction in the battery mass. This is because the power needed to accelerate to the fixed rotation speed reduces if a longer runway is available, and, as mentioned before, the battery is sized by its power requirement at the chosen design point of the FC-ATR 72. Through the snowball effect the MTOM and therefore the fuel mass are affected as well. When considering longer distances, the situation changes. After around 1500 m, the distance stops having an effect on the battery mass. In fact, at this point, the battery mass in terms of the energy becomes higher than that needed for power. As no other components are sized by the TO requirement, it stops having an effect on the MTOM as well. Note that the TO phase is only taken into account in the power loading computation and not the mission analysis, as can be seen in Table 4.4. If the latter was the case then a slight increase in all

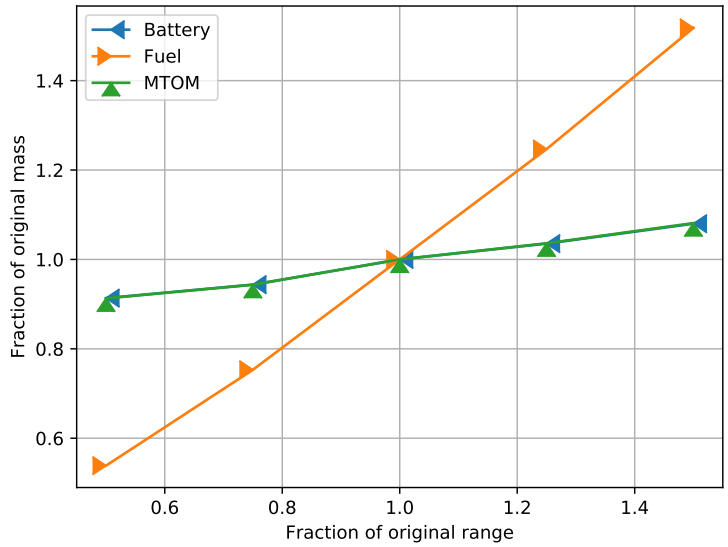

Figure 4.12: Effect of the design cruise range on the battery & fuel masses and the MTOM.

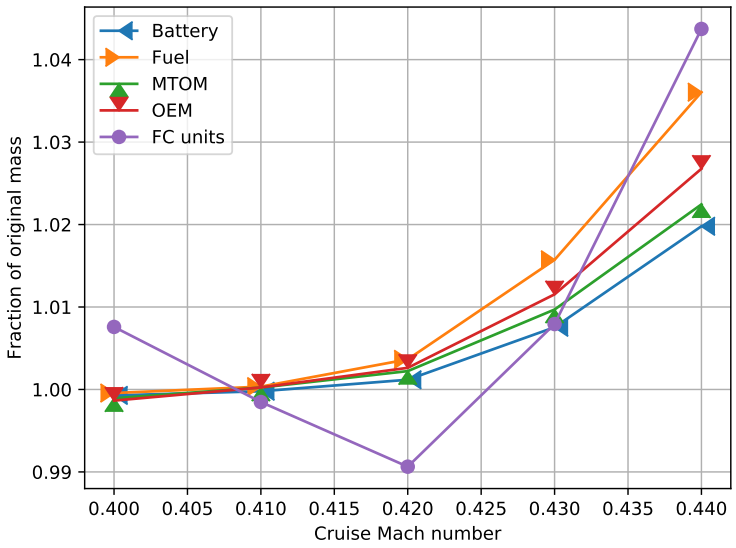

Figure 4.13: Effect of the cruise Mach number on various mass figures. The original Mach number is equal to 0.408.

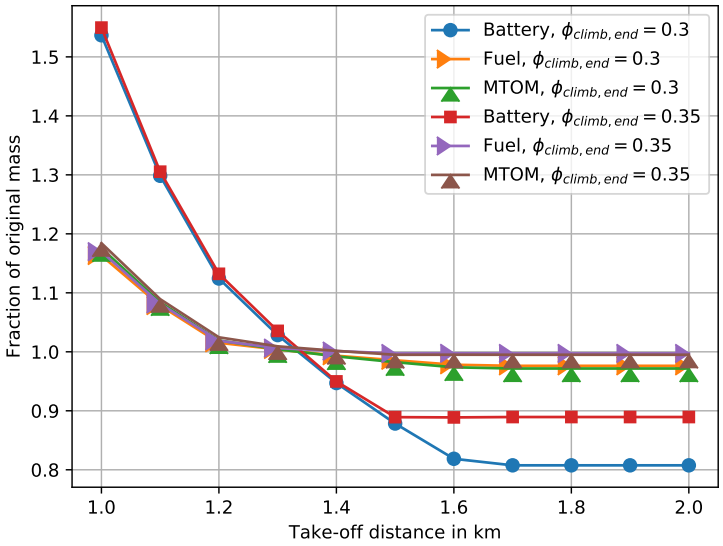

Figure 4.14: Effect of the take-off distance on the battery & fuel masses and the MTOM, plotted for two different top-of-climb supplied power ratios ($\Phi_{climb,end}$). The original distance is 1333 m.

masses would still be visible, as some fuel would be consumed during that very short phase of the flight.

Figure 4.14 shows the resulting masses at two different values for $\Phi_{climb,end}$. If this value is increased, then the battery takes over a larger portion of the power towards the end of the mission analysis climb phase. In the first half of the figure, this has no effect on the battery mass as this is sized by the TO requirement in terms of its power loading. In the second half, where the battery is sized by its energy from the mission analysis, it does make a difference. This then also causes a difference in MTOM and fuel mass. The results from this sensitivity study illustrate one of the main difficulties that arise in the optimisation of such a complex propulsion system. One might initially start focussing on a certain set of input parameters but as the optimisation advances, some of these parameters might stop having an effect, which would then require manual intervention to keep converging towards an optimum. Even bigger changes in the logic of the sizing, such as the battery being sized either by its power or energy, can also happen. A proper numerical optimisation will therefore have to consider all input parameters, which will make it a very large problem.

4.3.3. Effect of the Cruise Altitude on the Entire Aircraft

Although the effect of the cruise altitude was already examined on the level of the system in Figure 3.14, it does merit a short investigation in the context of the complete aircraft. Its effect is shown in Figure 4.15. Around the original value of 7 km, all masses increase, mainly due to a higher compressor mass. However, at lower altitudes, the masses show the opposite trend. The reason for this remains to be considered in detail in the future. However, one possibility is an initial increase in aerodynamic efficiency of the aircraft with a reduction in air density.

Not yet considered in this section are the electric motors. As can be seen in Figure 4.4c, they are sized by the OEI balked landing constraint. As the electric motors (EM2) are almost at the end of the propulsion chain (see Figure 3.11), a change in the power split between different sources does not have any effect. Instead, only a change in the absolute value of the propulsive power, mainly through a change in the corresponding constraint in the power loading graph would change the component mass. However, the parameters of this constraint (such as the required climb rate), are given by the certification specifications (in this case CS-25) and can therefore not be changed by the designer.

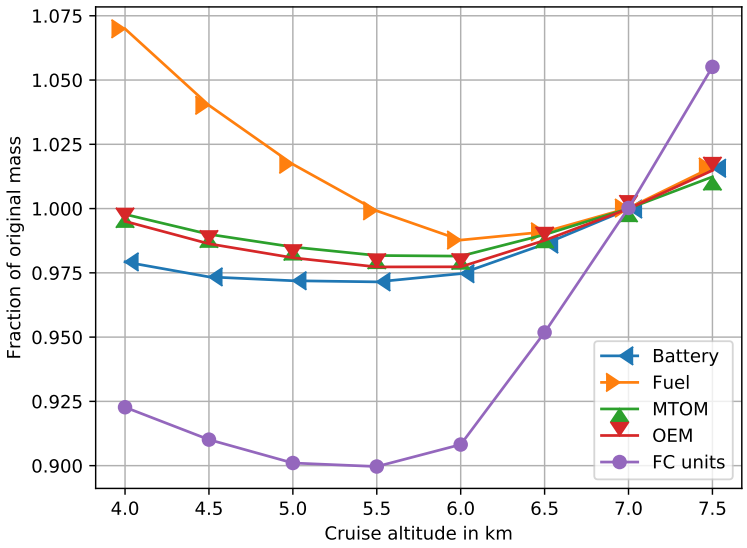

Figure 4.15: Effect of the cruise altitude on various mass figures, determined at the level of the complete aircraft. The original altitude is equal to 7km.

5

Conclusions & Recommendations

This final part of the thesis provides the opportunity to reflect on the development of the methods as well as the results obtained from their application. First, various conclusions are made regarding the sizing study and the sensitivity studies in section 5.1, mainly in connection with the research questions. This is followed by a number of recommendations for improvements and further developments in section 5.2.

5.1. Conclusions

The aim of this thesis project was to address some of the deficiencies in the current state of research into the sizing and design of FC aircraft by proposing a new set of methods for the application in a preliminary aircraft sizing process. The central deficiency, on which the main focus was placed, is expressed in the first research question: how can the accuracy of the weight estimation be improved? The answer consists of a number of different aspects, all of which were demonstrated in the set of methods proposed here. Firstly, it is necessary to zoom in further on the system, i.e. to go to the level of the subsystems, instead of just seeing the FC system as a black box with a given specific power. Secondly, it is necessary to rely mostly on physics, since there is essentially no statistical data as no such commercial aircraft have flown. Thirdly, it is important to note that at this level, the mass estimation becomes entangled with that of the performance, meaning that the latter must be included within the same set of methods as well. Fourthly, at least initially, certain choices must be made for the layout of the system and the type of components to be considered, as a FC system can take many different shapes and forms, especially when considering the placement on the aircraft.

At the time of writing, sizing approaches with these characteristics did exist, but only with regard to single parts of the system. Some of these were reused in chapter 3. In other research papers, only specific aircraft were considered or approaches were taken which do not agree with the aspects above, thereby forming the research gap. Therefore, considering the state of research at the time of the literature study phase of this thesis project, this is, to the author's best knowledge, the first instance of such as set of general methods presented in open literature. The focus here was not on the development of new theory or completely new single models, but rather on showing how existing knowledge can be effectively combined, taking into account the larger picture of the application to an aircraft sizing process.

Considering the contribution to research, a mere proposal does not suffice. An equally important part is the application of the proposed methods, in order to prove their suitability and to demonstrate their capabilities. In this case, it is also required in order to answer the second and the third research question. The first part of the application consisted of a sizing study using an existing regional turboprop aircraft as a reference. It was shown that the propulsion system model can be used within a complex aircraft sizing environment and that the main characteristics of the results, such as the specific power of the FC system, meet the expectations. The integration within such an environment is especially interesting, as it enables a more detailed consideration of the snowball effect. For instance, the effect of the hydrogen tank on the overall aircraft could be considered not just in terms of the fuselage stretch,

but also the associated increases in empty weight and drag, leading to a higher MTOM and power requirement. Also, a larger level of detail could be achieved in the results, especially considering the subsystems. Similarly, more detailed input conditions such as the cruise altitude and speed could be considered, which would not be possible if a simple approach such as a constant specific power was used. Furthermore, this is simply an interesting example for the application of this new technology, as such an aircraft will most likely be one of the first FC powered airliners, in terms of the number of passengers and the range.

The second part of the application of the models consisted of sensitivity studies, first applied only to the FC system model and later to the complete aircraft sizing procedure. The first goal of this part was to show the added value of this modelling approach. Studies such as those presented here, for instance regarding the effect of various atmospheric conditions on the mass distribution of the system, were not previously possible. The compressor pressure ratio β was identified as one of the most critical inputs, as it directly influences the result in two ways: through the compressor mass as well as its power requirement, which are both significant. It is interesting to note that performance-wise, providing less than sea-level pressure to the stacks might be beneficial. Beyond these concrete results, some broader statements about this new type of aircraft could be made following these results. For instance, it was shown that the range is much less critical than for propulsion systems, which rely on batteries as the only power source. Instead, the power required during various flight phases drives the design, mainly through the weight of the propulsion system. This underlines the increased importance of this mass parameter on the aircraft level, as compared to conventional, gas-turbine-powered designs.

So far, most conclusions from this thesis project are directly in relation to the research questions and the proposed set of methods. Following the development of the latter, their integration into an aircraft sizing environment was performed, having made the choice for the in-house Matlab tool called the Initiator. Although this is not of general scientific relevance, it should be mentioned that, time-wise, this implementation process accounts for a large amount of the work that was done. Most notably, this presents the first time that a FC was used in the Initiator. Beyond this, minor improvements and bugfixes were made during the coding process, presenting another valuable contribution to this research tool which is in continuous development at the faculty. In particular, one significant problem with respect to a missing battery mass in one of the MTOM summations of the hybrid branch was uncovered and fixed.

To conclude, in this thesis, a set of methods was presented from which a model was developed, which was then successfully applied to various sizing problems. The initial research questions were addressed, and additional insights were gained into the behaviour of FC aircraft during the design process. Not only does this form a starting point for further work on such propulsion systems within the Initiator, it can also be seen as a contribution to research in general, being one of the first generalised, physics based approaches to the sizing of a FC propulsion system.

5.2. Recommendations

Although the development of the model and the subsequent integration were successful and interesting results were ultimately obtained, many simplifying assumptions were introduced. Therefore, many improvements can still be made in future iterations of the modelling approach. Considering the stack, both the mass and the performance modelling can be improved in several ways. Firstly, some of the constants used in the former should be transformed into variables, such as for example the thickness of the endplates, which could be expressed as a function of the cell area or the number of cells, based on a database of existing designs. As already proposed, the bolts should be sized structurally, for which a way to determine the required mechanical pressure on the stack must be found. Furthermore, regarding the performance, a more detailed voltage loss model should be added to the polarization model. Despite extensive search, no analytical models could be found which express these losses as a function of the inlet conditions. Instead, reliance on better experimental data might be the way forward. In any case, this would allow a more flexible choice of the compression ratio β.

Similarly, a suitable loss model should be found for the centrifugal compressor. According to an expert who was consulted during the development, this is an active area of research. Furthermore, a more detailed consideration of the electric motor and the bearing assembly should be included. An interesting option to include in the model as an alternative to the EM would be to drive the compressor by the exhaust gasses. This might reduce the mass of the system, but would increase its complexity. Regarding the other BOP components, the internal pressure losses or drag should be considered more in detail, as already proposed for the heat exchanger in the original paper that was used as a reference. Regarding the humidifier, the iterational process shown by the original authors should be implemented as well. Finally, in all cases, constants such as the material thicknesses should be considered in detail.

Regarding the FC engines, the most important improvement will be to determine their physical design & layout, i.e. how the different subsystems are arranged within the nacelles. Fortunately, the geometric design of each subsystem follows from its mass modelling. Also, the Initiator already contains such capabilities for each part type. Multiple reasons exist for this improvement. Most importantly, it would allow a determination of the parasitic drag, given the frontal and wetted areas. This is currently completely omitted. It would also allow a more detailed consideration of their placement on the aircraft, for instance w.r.t. to the distance to the ground. Moreover, it could enable more advanced studies from a knowledge-based engineering perspective, such as an automated computational fluid dynamics analysis within the main sizing loop that would be facilitated by the existing 3D model. Next to this, additional subsystems, such as a voltage converter or a hydrogen recuperation system, or other types of the same subsystems, such as evaporative cooling, might be interesting to introduce.

The biggest improvement to be made on the level of the aircraft sizing process is the development of a new engine type in the Initiator as currently, the gas-turbine code of the hybrid branch is ”hijacked” for this purpose. Furthermore, it would be interesting to attempt an automatisation of the optimisation process, mainly in application to the power control parameters or important subsystem design parameters such as β or the voltage oversizing factor. In connection to this, some of the specific design choices such as requiring the compressor to provide sea-level pressure should be relaxed. In that case, however, the FC system model would have to use more than one flight phase as an input. Already included in the Initiator are various Class 2.5 methods, which should be enabled for an FC aircraft sizing study. It would be especially interesting to consider the influence of the lack of fuel in the wings in combination with the heavier engines on the structural weight of the wing. Two other important components are the hydrogen tank and battery, which are currently not yet included in the Initiator as separate parts. Especially regarding the latter, this would allow a more detailed consideration of the CG as well as the physical integration in the aircraft. Finally, with respect to real-world sizing scenarios, multiple input missions should be used.

When implementing most of the improvements and extensions mentioned here above, one most keep in mind the balance between the generality of the method and its level of detail. Increasing the latter will most likely require the further specialisation to CS-25 aircraft, meaning that the development of a separate modelling approach for other certification classes might be interesting. Another general remark is that the validation should be improved. Although this is currently challenging, it will become easier as more research is done and the first aircraft are introduced in the market. Finally, sizing studies of different categories should be made, especially of medium-range single aisle or smaller aircraft in the range of 20 seats, in addition to other types of sensitivity studies that were not considered here.

A

Additional Results for the Conventional ATR 72 Sized in the Initiator

This appendix contains certain additional results from the sizing of the conventional ATR 72-600 in the Initiator. These results are not directly (or at least not extensively) used in the chapters above and are therefore just presented here, for further reference or comparisons.

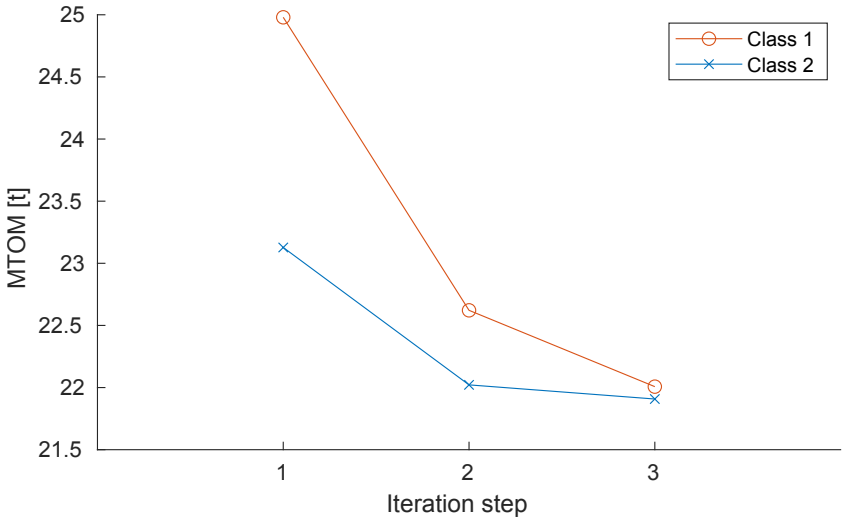

Figure A.1: Convergence history of the conventional ATR 72 sized in the Initiator, in terms of its MTOM. The corresponding graph for the FC-ATR 72 is shown in Figure 4.1. Note that here the slope is negative, instead of positive.

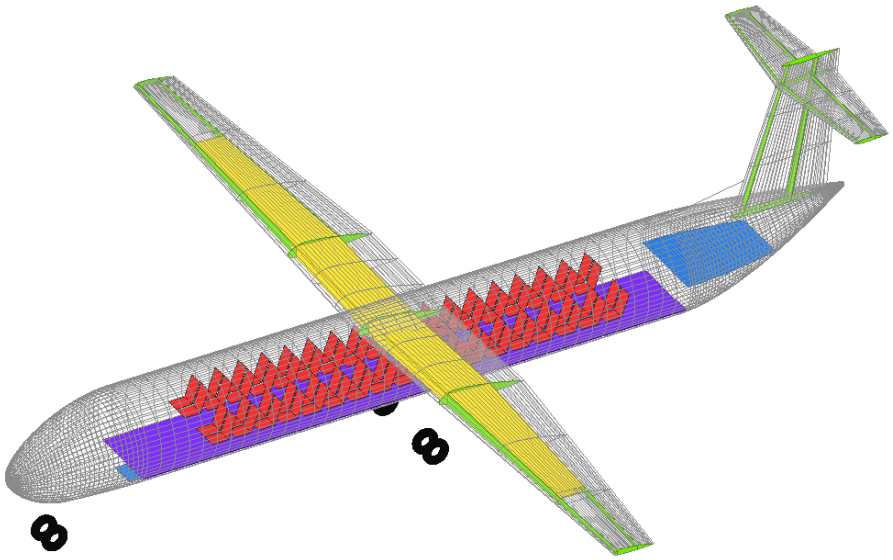

Figure A.2: Isometric view of the conventional ATR 72 sized in the Initiator. The corresponding rendering for the FC-ATR 72 is shown in Figure 4.2. Note that the tailcone starts directly after the cabin, as no fuel tank is present in the fuselage. Instead, the kerosene tank is now visible in the wing. Furthermore, just as in Figure 4.2, the engines are not shown.

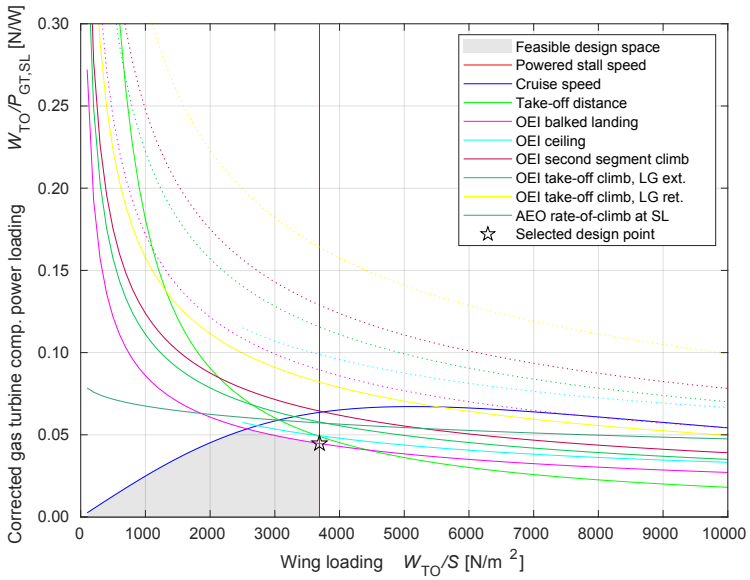

Figure A.3: Corrected gas turbine component power loading graph of the conventional ATR 72 sized in the Initiator. The corresponding graph for the FC-ATR 72 is shown in Figure 4.4a. In this case, the only correction applied to the constraints is due to the power lapse of the gas turbine, i.e. its reduction in power with altitude.

Bibliography

[1] B. Graver, K. Zhang, and D. Rutherford. *CO_2 emissions from commercial aviation, 2018*. [ICCT working paper]. 2018. URL: https://theicct.org/sites/default/files/publications/ICCT_CO2-commercl-aviation-2018_20190918.pdf.

[2] D. S. Lee et al. "The contribution of global aviation to anthropogenic climate forcing for 2000 to 2018". In: *Atmospheric Environment* 244 (Sept. 2020), p. 117834. ISSN: 18732844. DOI: 10.1016/j.atmosenv.2020.117834.

[3] Fuel Cells and Hydrogen 2 Joint Undertaking. *Hydrogen-powered aviation A fact-based study of hydrogen technology, economics, and climate impact by 2050*. July 2020. DOI: 10.2843/766989.

[4] Daniel Juschus. *Literature Study Report - Modular PEM Fuel Cell System Weight Estimation Method for Initial Aircraft Design Phases*. Delft University of Technoloy. Unpublished. Jan. 2021.

[5] P Zhou, C W Wu, and G J Ma. "Influence of clamping force on the performance of PEMFCs". In: *Journal of Power Sources* 163.2 (2007), pp. 874–881. ISSN: 03787753. DOI: 10.1016/j.jpowsour.2006.09.068.

[6] Joseph W. Pratt, Jacob Brouwer, and G. Scott Samuelsen. "Performance of proton exchange membrane fuel cell at high-altitude conditions". In: *Journal of Propulsion and Power* 23.2 (2007), pp. 437–444. ISSN: 15333876. DOI: 10.2514/1.20535. URL: https://escholarship.org/uc/item/2g62m8k9.

[7] A. Wiartalla et al. "Compressor expander units for fuel cell systems". In: vol. 109. 2000, pp. 484–488. DOI: 10.4271/2000-01-0380.

[8] Benjamin Blunier and Abdellatif Miraoui. "Air management in PEM fuel cells: State-of-the-art and prospectives". In: *International Aegean Conference on Electrical Machines and Power Electronics and Electromotion ACEMP'07 and Electromotion'07 Joint Conference* (Sept. 10–12, 2007). Bodrum, Turkey, 2007, pp. 245–254. ISBN: 1424408911. DOI: 10.1109/ACEMP.2007.4510510.

[9] Dragan Kožulović. "Heat Release of Fuel Cell Powered Aircraft". In: *Proceedings of Global Power and Propulsion Society* (Sept. 7–9, 2020). Chania, Greece, Sept. 2020. DOI: 10.33737/gpps20-tc-99.

[10] Guangsheng Zhang and Satish G Kandlikar. "A critical review of cooling techniques in proton exchange membrane fuel cell stacks". In: *International Journal of Hydrogen Energy* 37.3 (2012), pp. 2412–2429. ISSN: 03603199. DOI: 10.1016/j.ijhydene.2011.11.010.

[11] A. Fly and R. H. Thring. "A comparison of evaporative and liquid cooling methods for fuel cell vehicles". In: *International Journal of Hydrogen Energy* 41.32 (Aug. 2016), pp. 14217–14229. ISSN: 03603199. DOI: 10.1016/j.ijhydene.2016.06.089.

[12] Ryan Huizing et al. "Design methodology for membrane-based plate-and-frame fuel cell humidifiers". In: *Journal of Power Sources* 180.1 (May 2008), pp. 265–275. ISSN: 03787753. DOI: 10.1016/j.jpowsour.2008.01.046.

[13] Yafei Chang et al. "Humidification strategy for polymer electrolyte membrane fuel cells – A review". In: *Applied Energy* 230 (Nov. 2018), pp. 643–662. ISSN: 03062619. DOI: 10.1016/j.apenergy.2018.08.125.

[14] Mengbo Ji and Zidong Wei. "A review of water management in polymer electrolyte membrane fuel cells". In: *Energies* 2.4 (2009), pp. 1057–1106. ISSN: 19961073. DOI: 10.3390/en20401057. URL: www.mdpi.com/journal/energies.

[15] Dries Verstraete, Luigi Cazzato, and Giulio Romeo. "Preliminary design of a fuel-cell-based hybrid-electrical UAV". In: *28th Congress of the International Council of the Aeronautical Sciences 2012, ICAS 2012* (Sept. 23–28, 2012). Vol. 1. Brisbane, Australia, Jan. 2012, pp. 422–431. URL: https://www.icas.org/ICAS_ARCHIVE/ICAS2012/ABSTRACTS/654.HTM.

[16] Mohamed Gadalla and Sayem Zafar. “Analysis of a hydrogen fuel cell-PV power system for small UAV”. In: *International Journal of Hydrogen Energy* 41.15 (Apr. 2016), pp. 6422–6432. DOI: 10.1016/j.ijhydene.2016.02.129.

[17] Taek Hyun Oh. “Conceptual design of small unmanned aerial vehicle with proton exchange membrane fuel cell system for long endurance mission”. In: *Energy Conversion and Management* 176 (Nov. 2018), pp. 349–356. ISSN: 01968904. DOI: 10.1016/j.enconman.2018.09.036.

[18] Lorenzo Trainelli et al. *Sizing and Performance of Hydrogen-Driven Airplanes*. Rome, Italy, 2019. URL: https://www.researchgate.net/publication/336025468.

[19] Mark D. Guynn, Joshua E. Freh, and Erik D. Olson. “Evaluation of a Hydrogen Fuel Cell Powered Blended-Wing-Body Aircraft Concept for Reduced Noise and Emissions”. In: *NASA technical memoranda* February (2004). URL: https://ntrs.nasa.gov/citations/20040033924.

[20] Thomas Kadyk et al. “Analysis and Design of Fuel Cell Systems for Aviation”. In: *Energies* 11.2 (2018), pp. 1–15. ISSN: 19961073. DOI: 10.3390/en11020375.

[21] Blake A. Moffitt et al. “Reducing Uncertainty of a Fuel Cell UAV through Variable Fidelity Optimization”. In: *7th AIAA ATIO Conf, 2nd CEIAT Int'l Conf on Innov and Integr in Aero Sciences,17th LTA Systems Tech Conf; followed by 2nd TEOS Forum* (Sept. 18–20, 2007). Belfast, Northern Ireland, 2007. DOI: 10.2514/6.2007-7793.

[22] Davide Comincini. *Modular approach to hydrogen hybrid-electric aircraft design*. MSc thesis. Politecnico Milano. Dec. 2017. URL: https://www.politesi.polimi.it/handle/10589/143966.

[23] Thomas Kadyk et al. “Design of fuel cell systems for aviation: Representative mission profiles and sensitivity analyses”. In: *Frontiers in Energy Research* 7:35 (Apr. 2019), p. 35. ISSN: 2296598X. DOI: 10.3389/fenrg.2019.00035.

[24] R. O'Hayre et al. *Fuel Cell Fundamentals*. Wiley, 2016. ISBN: 9781119113805.

[25] A.L. Dicks and D.A.J. Rand. *Fuel Cell Systems Explained*. Wiley, 2018. ISBN: 9781118706978.

[26] Stine Søndergaard. “Pressurised High Temperature Polymer Electrolyte Membrane Fuel Cells for H2/O2 Operation”. PhD thesis. Technical University of Denmark, 2015.

[27] Kivanc Karacan et al. “Investigation of formability of metallic bipolar plates via stamping for light-weight PEM fuel cells”. In: *International Journal of Hydrogen Energy* 45.60 (Feb. 2020), pp. 35149–35161. ISSN: 03603199. DOI: 10.1016/j.ijhydene.2020.01.251.

[28] Shahram Karimi et al. “A Review of Metallic Bipolar Plates for Proton Exchange Membrane Fuel Cells: Materials and Fabrication Methods”. In: *Advances in Materials Science and Engineering* 2012 (2012), p. 22. DOI: 10.1155/2012/828070.

[29] S. Asghari, M. H. Shahsamandi, and M. R. Ashraf Khorasani. “Design and manufacturing of end plates of a 5 kW PEM fuel cell”. In: *International Journal of Hydrogen Energy* 35.17 (2010), pp. 9291–9297. ISSN: 03603199. DOI: 10.1016/j.ijhydene.2010.02.135.

[30] Mostafa Habibnia, Mohammadreza Shirkhani, and Peyman Ghasemi Tamami. “Optimization of proton exchange membrane fuel cell's end plates”. In: *SN Applied Sciences* 2.8 (2020). ISSN: 2523-3963. DOI: 10.1007/s42452-020-3177-2.

[31] Tapobrata Dey et al. “Study of PEM Fuel Cell End Plate Design by Structural Analysis Based on Contact Pressure”. In: *Journal of Energy* 2019 (2019), pp. 1–11. ISSN: 2356-735X. DOI: 10.1155/2019/3821082. URL: https://doi.org/10.1155/2019/3821082.

[32] M. Gambini and M. Vellini. *Turbomachinery: Fundamentals, Selection and Preliminary Design*. Springer Tracts in Mechanical Engineering. Springer International Publishing AG, 2020. ISBN: 9783030512996.

[33] Cheng Xu and Ryoichi S. Amano. “Empirical design considerations for industrial centrifugal compressors”. In: *International Journal of Rotating Machinery* 2012 (2012). ISSN: 1023621X. DOI: 10.1155/2012/184061.

[34] Giuseppe Onorato. *Fuel Tank Integration for Hydrogen Airliners*. MSc thesis. Delft University of Technology. 2021. URL: https://repository.tudelft.nl/islandora/object/uuid%3A5700b748-82c6-49c9-b94a-ad97c798e119.

[35] Reynard de Vries, Malcom T. Brown, and Roelof Vos. “A preliminary sizing method for hybrid-electric aircraft including aero-propulsive interaction effects”. In: *2018 Aviation Technology, Integration, and Operations Conference*. 2018. ISBN: 9781624105562. DOI: 10.2514/6.2018-4228.

[36] Thomas H. Bradley et al. “Development and experimental characterization of a fuel cell powered aircraft”. In: *Journal of Power Sources* 171.2 (2007), pp. 793–801. ISSN: 03787753. DOI: 10.1016/j.jpowsour.2007.06.215.

[37] Haruki Tsuchiya and Osamu Kobayashi. “Mass production cost of PEM fuel cell by learning curve”. In: *International Journal of Hydrogen Energy* 29.10 (2004), pp. 985–990. ISSN: 03603199. DOI: 10.1016/j.ijhydene.2003.10.011.

[38] K. Jayakumar et al. “Cost-benefit analysis of commercial bipolar plates for PEMFC’s”. In: *Journal of Power Sources* 161.1 (Oct. 2006), pp. 454–459. ISSN: 03787753. DOI: 10.1016/j.jpowsour.2006.04.128.